CHALMERS
UNIVERSITY OF TECHNOLOGY

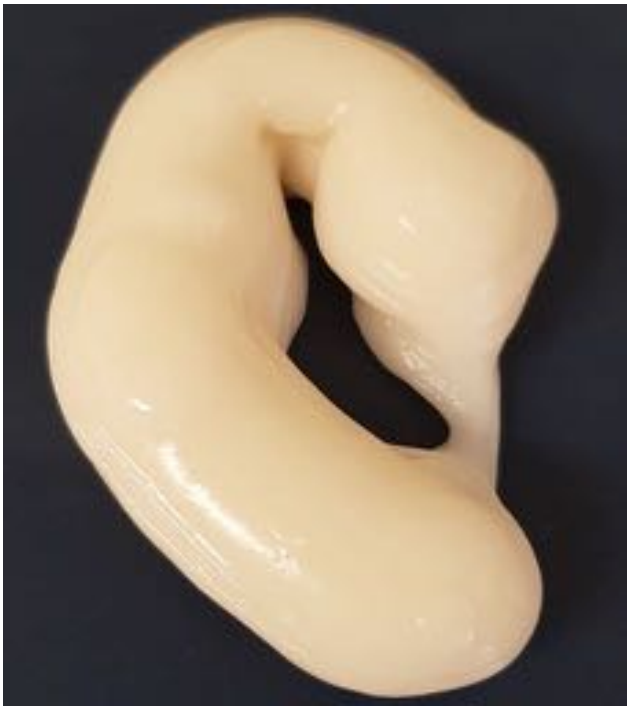

3D Bioprinting Meniscus

for Future Tissue Replacement in Osteoarthritis Affected Knee Joints

Master's Thesis in Master's Programme MPBIO

IDA PETTERSSON
AMANDA OLSSON WIDJAJA

Department of Chemistry and Chemical Engineering
Department of Biology and Biological Engineering
CHALMERS UNIVERSITY OF TECHNOLOGY
Gothenburg, Sweden 2020

Master's thesis 2020

3D Bioprinting Meniscus

for Future Tissue Replacement in Osteoarthritis Affected Knee Joints

IDA PETTERSSON
AMANDA OLSSON WIDJAJA

CHALMERS
UNIVERSITY OF TECHNOLOGY

Department of Chemistry and Chemical Engineering
Department of Biology and Biological Engineering
Institute of Biomedicine at Sahlgrenska Academy
Department of Clinical Chemistry and Transfusion Medicine, University of Gothenburg
Chalmers University of Technology
Gothenburg, Sweden 2020

3D Bioprinting Meniscus
for Future Tissue Replacement in Osteoarthritis Affected Knee Joints

Supervisor: Stina Simonsson, Department of Clinical Chemistry and Transfusion Medicine, University of Gothenburg
Examiner: Paul Gatenholm, Department of Chemistry and Chemical Engineering at Chalmers University of Technology in Gothenburg, Sweden

Master's Thesis 2020
Department of Chemistry and Chemical Engineering at Chalmers University of Technology
Department of Biology and Biological Engineering at Chalmers University of Technology
Institute of Biomedicine at Sahlgrenska Academy
Department of Clinical Chemistry and Transfusion Medicine,
University of Gothenburg
Chalmers University of Technology
SE-412 96 Gothenburg
Telephone +46 31 772 1000

Approved June 17, 2020

Paul Gatenholm, Professor

Cover: 3D bioprinted full scale meniscus, bioprinted with a bioink composed of nanofibrillated cellulose and alginate.

Typeset in LaTeX
Printed by Chalmers Reproservice
Gothenburg, Sweden 2020

Acknowledgements

We would like to express our special thanks of gratitude to our supervisor at the Sahlgrenska Academy, Stina Simonsson, for all the inspiring ideas and invaluable expertise. Secondly, we would also like to thank Carl Lindahl, Narmin Bigdeli, Josefine Ekholm, Linnea Andreasson, Marianne Jonsson and Camilla Brantsing for your guidance, advice, and inclusion within the team. We also want to express our gratitude to Anna Ström at Chalmers University of Technology for assistance with the measurements of the rheological properties, that were results of great importance. Lastly, a very special thank you to Professor Paul Gatenholm for introducing the both of us to Tissue Engineering thus 3D Bioprinting, for the encouragement throughout the project and for being our examiner.

Ida Pettersson, Amanda Olsson Widjaja, Gothenburg, June 2020

Abstract

Progressive cartilage defects in human knee joints are a worldwide health issue that exposes a great burden on society as well as on single individuals. Sudden traumas to the knees can induce tears in the structures of the joints such as the articular cartilage and the meniscus. Lesions in the cartilage tissue of the knee joints have a high probability to eventuate in osteoarthritis (OA). The emerging technique of 3D bioprinting tissue is a novel approach for cartilage repair and regeneration. The choice of bioink and cell type are important factors that considerably impact the resulting cartilage repair potential after the process of 3D bioprinting. Induced pluripotent stem cells possess the ability to differentiate into almost any cell type and their potential in future regenerative medicine is of great interest.

The present study has investigated the possibility of 3D bioprinting chondrocyte-derived human induced pluripotent stem (iPS) cells into meniscus structures with initiated cartilage regeneration. A combination of nanofibrillated cellulose (NFC) and alginate (A) was used as bioink. At first, the bioink was subjected to optimization to augment printing properties and cell viability during and after bioprinting. The composition of nanofibrillated cellulose and alginate originated from a ratio of 60/40 NFC/A (% w/w) that was compared with one ratio of 48/52 NFC/A (% w/w) and one ratio of 80/20 NFC/A (% w/w). The optimization of bioink involved measurements of printability, rheology, and cell viability.

The formation of microtissues enabled differentiation of iPS cells toward extracellular matrix (ECM) producing cells prior to 3D bioprinting. 3D bioprinted menisci, as well as cultured microtissues, were analyzed with LIVE/DEAD assay, immunohistochemical analysis, and quantitative reverse transcription polymerase chain reaction (qRT-PCR). The work also comprised an *in vivo* assay of 3D bioprinted constructs transplanted subcutaneously in mice to enable the evaluation of tissue formation in a realistic milieu.

Induced pluripotent stem cells further modified to express green fluorescence protein under the aggrecan promotor have been subjected to a screening of a library of small Food and Drug Administration (FDA) approved molecules. Changes in intensity indicated induction or inhibition of the synthesis of aggrecan. Moreover, the screening highlighted molecules included in the induction or inhibition of aggrecan production. These molecules will be subjected to further investigations to evaluate their possible contribution in future OA-treatments.

The prevailing work demonstrates the feasibility of utilizing microtissues formed by iPS cells for the 3D bioprinting of cartilage tissue. The culturing of iPS cells as microtissues has proven to induce differentiation and synthesis of components included in the ECM, both *in vitro* and *in vivo*. Simultaneously, the study has included a comparison of three bioinks that resulted in an optimized protocol for the production of the bioink composed of 60/40 NFC/A (% w/w). This optimized bioink fulfilled the requirements of being printable while supporting cell viability.

Keywords: Alginate, Articular Cartilage, Bioink, Induced Pluripotent Stem Cells, Meniscus, Nanofibrillated Cellulose, Osteoarthritis, Screening, 3D Bioprinting.

Contents

1
Introduction

Running, walking, standing, and even sitting down with the legs bent are movements taken for granted by the majority. For people with lesions in the cartilaginous tissue of the knee joints, these motions may be impaired and associated with great pain. In the knee joint, bones, tendons, and ligaments are united to provide fully functional flexion and extension of the leg. To further promote pliable mobility, articular cartilage and menisci are situated between the bones, offering smooth movement and cushioning effects in the knee.

Osteoarthritis (OA) is a degradable joint disease that starts and gradually worsens. The meniscus, as well as the articular cartilage are tissues situated in the knee joint that are correlated to OA. Age, weak muscles, obesity, joint injuries and wear and tear are factors that can contribute to OA (Artros.org, 2019). The disease causes a cartilage breakdown that can result in swollen joints with impaired flexion and extension and eventually serious mobility difficulties (Artros.org, 2019). Cartilage is avascular and has a poor ability to repair itself, thus the self-healing of cartilage lesions is restricted (Artros.org, 2019). As the degradation of cartilage proceeds, bones will eventually start to rub against each other. This abrasive wear can cause a breakdown of bones that results in patients suffering and enduring severe pain (Arthritis Foundation, 2017).

OA is the most common joint disease worldwide. There are 800,000 patients suffering from OA in Sweden today and one out of four persons over 45 years old are estimated to suffer from the disease (Artros.org, 2019). To maintain a healthy weight and exercise can help to prevent OA but the disease can not be cured nor can the already damaged cartilage be restored through these actions, they will only help to prevent further complications (Artros.org, 2019).

Currently, there are methods that can treat OA to some extent. The joint with damaged cartilage can be artificially replaced or cartilage-like tissue can be induced with microfracture treatment. Autologous Chondrocyte Implantation (ACI) and Matrix-associated Chondrocyte Implantation (MACI) are two methods to repair damaged cartilage with the patient's own cells (Gille, Behrens, Schulz, Oheim, & Kienast, 2016). With ACI healthy chondrocytes are obtained from the patient. The cells are cultured and thereafter re-implanted to the site of the cartilage lesion (Gille et al., 2016). MACI is an analogous method but more advanced, as the chondrocytes are seeded on a collagen layer of a matrix (Gille et al., 2016). The choice of treatment is dependent on what technique that is thought to suit the patient (Strauss,

Barker, Kercher, Cole, & Mithoefer, 2010).

Similarly to articular cartilage, the meniscus is also seriously affected in the case of OA. The meniscus plays a vital role in sustaining a proper function of the knee joint. It acts as a shock absorber that distributes the compressive load applied from the upper body. Further, it provides smooth movement and reduces the friction between the femur and the tibia bone (Makris, Hadidi, & Athanasiou, 2011). Meniscal injuries are well distributed among all age groups. Sports traumas are a common cause within young and active people whereas the elderly are at risk because of the wear and tear of cartilage that follows with old age (Doral, Bilge, Huri, Turhan, & Verdonk, n.d.). The number of people carrying a meniscal injury is high and these types of lesions are therefore also related to high costs. In Sweden, there are more than 30,000 meniscus surgeries performed yearly (Ortho Center Skåne, 2011). In the US about 170,000 of all the orthopedic surgeries involve surgical repair of the meniscus, thus arthroscopic surgery for a meniscus tear is one of the most common surgical procedures performed in the US today (Kawata et al., 2018). Similar to other cartilage structures, the meniscus has a poor self-repair capacity, particularly in its inner parts where the blood supply is non-existent (Doral et al., n.d.).

To heal meniscal injuries there are a few surgical treatments available; meniscectomy (partial or total), meniscal repair, and meniscal reconstruction (Doral et al., n.d.). Total meniscectomy was performed more frequently up until its strong correlation to OA was established. Meniscal repair can be performed through arthroscopy and is an attempt to repair the meniscus, for instance with sutures. The outcome however varies and is highly dependent on the placement of the tear (Doral et al., n.d.). Meniscal reconstruction uses meniscal allograft transplantation (MAT) to replace tissue after total or partial meniscectomy. Also, scaffolds and collagen-based and cell-based implants are hot topics for meniscal reconstruction (Jarit & Bosco, 2010). As these novel techniques are still under development, further studies need to be executed to evaluate the clinical outcome of these types of reconstructions (Jarit & Bosco, 2010).

The choice of scaffold or implant is crucial for the healing process of a meniscal reconstruction. A promising technique to achieve personalized implants is to 3D bioprint a meniscus structure. 3D bioprinting is a technique where cells and a carefully selected bioink are utilized together to form tissue-like 3D-structures. With this method, it is possible to start with magnetic resonance imaging (MRI) to obtain an implant of a perfect fit for each individual patient. By choosing a bioink that is biocompatible and combining the bioink with induced pluripotent stem cells that have the capacity to differentiate into any cell type, there is a possibility to achieve an implant with initiated cartilage regeneration.

1.1 Objectives

The aim of the master thesis project is to 3D bioprint menisci and other cartilaginous tissues with initiated cartilage formation. Induced pluripotent stem (iPS) cells together with a bioink made of alginate and nanofibrillated cellulose (NFC) is the combination that composes the basis for bioprinting. Emphasis is on the optimization of the performance of the bioink as well as the 3D bioprinted structures where the cells have a high viability and produce the extracellular matrix specific for cartilage tissue. The project is executed as a step in the process of cartilage regeneration and repair.

Further, a library of FDA-approved molecules is screened with the expectation to find induction or inhibition of aggrecan production. Aggrecans are thought to be linked to cartilage degradation and OA. The aim of the screening is to work towards a possible cure for OA.

2

Theory

The knee is a complex joint that combines bones, ligaments, and tendons to provide flexion and extension of the legs as well as smooth body movement and stability. A fully functioning and healthy knee joint is crucial for proper knee mobility necessary to maintain everyday activities such as walking and standing. The following chapter gives an introduction to the structure of the knee, the articular cartilage, and the meniscus. Further, cartilage- and meniscal injuries and diseases, as well as possible treatments are discussed. Finally, some theory about 3D bioprinting and bioink requirements are provided.

2.1 Articular Cartilage Structure and Composition

The ends of the bones in diarthrodial joints are covered by a white and smooth connective tissue called articular cartilage. Articular cartilage has two major purposes; to distribute the compressive load that arises in the joint upon movement and to provide low motion friction between the bones (Roughley & Mort, 2014). Articular cartilage is, in fact, hyaline cartilage that is found on the articular surfaces of bones. It is composed of cartilage cells (chondrocytes) dispersed in an extracellular matrix (ECM) synthesized by the chondrocytes themselves. The main constituents of articular cartilage ECM are water, collagen type II and proteoglycans. Although in lesser amounts, non-collagenous proteins and other glycoproteins are also present (Sophia Fox, Bedi, & Rodeo, 2009). Combined, these components contribute to the mechanical performance of cartilage. The articular cartilage is fairly thin, only 2-4 mm, yet it can be divided into four zones; superficial, middle, deep, and calcified zone (Sophia Fox et al., 2009).

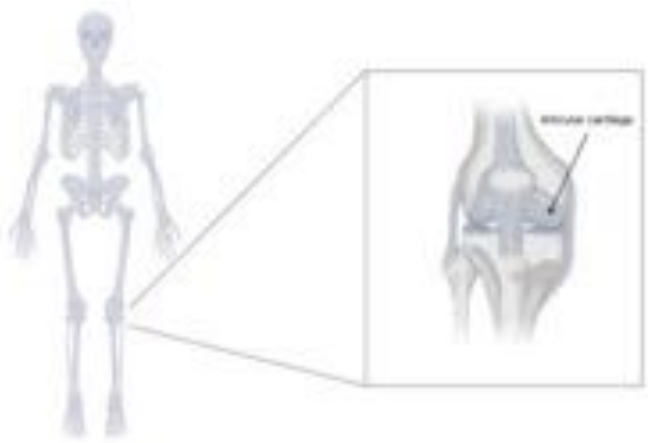

Figure 2.1: The ends of the bones in diarthrodial joints are covered with articular cartilage. Figure created with BioRender.com

2.1.1 Zonal Architecture of Articular Cartilage

The calcified zone is located adjacent to the subchondral bone and functions as a mechanical linkage between the bone and the cartilage (Sophia Fox et al., 2009). This area holds just a low number of chondrocytes compared to the other, more cell-dense zones. Further, the cells in this zone display hypertrophic characteristics which slightly distinguish them from other chondrocytes. With their hypertrophic features, the cells can produce calcified ECM and collagen type X which is short-chained collagen (Poole et al., 2001). Next to the calcified zone, anchored by collagen fibrils, lies the deep zone. In this region, collagen fibrils are arranged perpendicular to the articular surface with chondrocytes lined parallel to the fibrils (Gobbi & Lane, 2017, p. 88). The deep zone possesses a low cell and collagen quantity but an extensive concentration of proteoglycans. Due to the high proteoglycan content combined with the perpendicular positioning of collagen fibrils, the deep zone exhibits great resistance to compressing load (Gobbi & Lane, 2017, p. 88). Above the deep zone lies the middle (transitional) zone. In this zone, the cell density increases, the collagen fibrils are randomly organized and the chondrocytes hold a spherical morphology (Poole et al., 2001). The superficial zone, located closest to the articular surface, has collagen and chondrocytes arranged recumbent, along the surface (Sophia Fox et al., 2009). As the superficial zone is the first exposed to outer stresses, it functions to protect the deeper zones. Therefore it holds the capability to resist shear, tensile, and compressive strength (Poole et al., 2001).

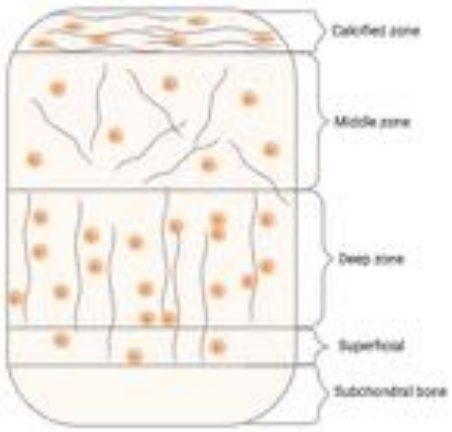

Figure 2.2: Zonal architecture of articular cartilage. Arrangement of collagen fibrils and chondrocytes in all layers. Figure created with BioRender.com

2.2 Meniscus Structure and Function

Within the knee joint, situated between the tibia and femur bones lies another cartilaginous tissue; the meniscus. The meniscus is in fact composed of two parts; the medial meniscus and the lateral meniscus. Both menisci are crescent-shaped but differ slightly in size and structure (Makris et al., 2011). The lateral meniscus is somewhat smaller than the medial meniscus, yet it covers a greater area of the tibia plateau (Makris et al., 2011). The meniscus consists of fibrocartilage with collagen type I as the major fibrous protein of the ECM, compared to articular cartilage where collagen type II is predominant (Gobbi & Lane, 2017, p. 74). The collagen fibers are aligned circumferentially throughout the central meniscus structure, as well as they are radially arranged in the outer periphery, towards the inner region (Gobbi & Lane, 2017, p. 340). The two alignments of the collagen fibers contribute to the tensile strength and radial stiffness of the meniscus (Gobbi & Lane, 2017, p. 340). The cell type varies depending on where in the meniscus the cells are situated. In the central meniscus, the cells are articular chondrocyte-like and produce mainly collagen type II and the proteoglycan aggrecan. Further to the periphery, the cells are fibroblast-like and produce fibrocartilage with collagen type I (Makris et al., 2011)(Sanchez-Adams & Athanasiou, 2012). Besides cells and ECM, the meniscus holds a high water content, namely around 72 % (Makris et al., 2011).

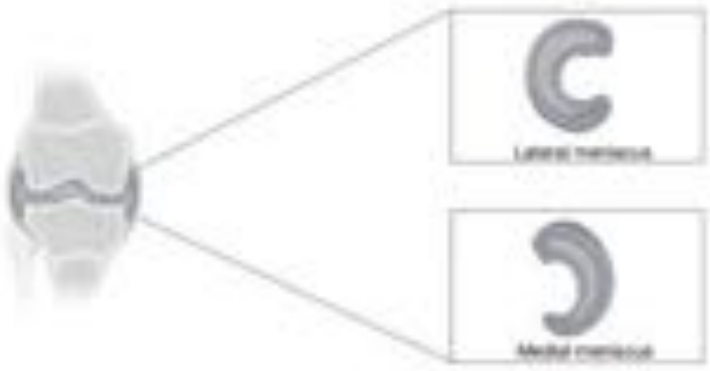

Figure 2.3: Lateral and medial meniscus located between the femur and tibia bone. Figure created with BioRender.com

2.2.1 Vascularization of the Meniscus

In early development, blood vessels are distributed throughout the entire meniscus. With time, the vascularization decreases, thus the inner center of an adult meniscus is avascular and blood vessels are only to be found in the outer parts (Makris et al., 2011)(Gobbi & Lane, 2017, p. 340). The peripheral, vascularized part of the meniscus is often referred to as the red-red zone. Here, nerves are also present and in combination with blood vessels, the outer part of the meniscus is able to self-repair when damaged (Gobbi & Lane, 2017, p. 340). The inner center has poor self-repair capacity because of its avascularity, allowing for severe complications in case of an injury in the inner parts (Makris et al., 2011). This avascular area is recognized as the white-white zone while the separating area in between the red and the white region is referred to as the red-white zone.

2.2.2 Function of the Meniscus

The meniscus plays a vital role in a proper biomechanical function of a knee. It mainly serves to moderate the forces impacting the knee. The compressive load applied from the upper body and through the femur bone is allocated over the meniscus hence increasing the contact area between the bones (Gobbi & Lane, 2017, p. 341). The meniscus thereby alleviates the tibia bone from extensive loading. The meniscus can be compared to a cushion that lies on the tibia plateau and act as a shock absorber to protect the bones from impact. Additionally, the meniscus has to withstand shear and tension forces to enable flexion and extension as well as provide stability to the knee (Gobbi & Lane, 2017, p. 341). Another important key function of the meniscus is to deliver lubrication and nutrition to the knee joint. Since articular cartilage is an avascular tissue, nutrients and oxygen can not be supplied

by the blood. Instead, the cartilage relies on nutrition and oxygen diffusion from the synovial fluid (Wang, Wei, Zeng, He, & Wei, 2013). When the meniscus is compressed, the synovial fluid is distributed to the articular cartilage and yields both nutrition and lubrication. Lubrication is a necessity to maintain a smooth movement of the knee joint (Makris et al., 2011).

2.2.3 Meniscal Injuries

An intact structure of both the lateral and medial parts of the meniscus is critical for a healthy knee joint. Any damage to the meniscus can lead to increased stress to the cartilage as the function of distributing load and act as a shock absorber is impaired (Gobbi & Lane, 2017, p. 339). Meniscal lesions can be either traumatic or degenerative where the former often arises due to a specific injury directed to the knee while the latter emerges over time (Gobbi & Lane, 2017, p. 344). Traumatic meniscal injuries affect people of all ages and are often the result of sports trauma where forceful twisting or hyperextension has occurred (Makris et al., 2011). Traumatic meniscal tears often contribute to pain, swelling, and locking of the knee and can eventually develop into a progressive joint dysfunction. Degenerative meniscal lesions, on the other hand, are not caused by a specific trauma directed at the knee joint. Instead, these tears are evolving over time (Gobbi & Lane, 2017, p. 344). The knee joint is subjected to extensive wear and tear and has to withstand massive load applied from the upper body. The constant wearing down of the knee joint is a possible cause for degenerative tears of the meniscus. Furthermore, people at middle-age and elder are most commonly affected by degenerative meniscal lesions (Gobbi & Lane, 2017, p. 345). Tears that emerge in the red-red zone are considered less complex compared to injuries in the white-white zone (Makris et al., 2011). Owing to the vascularization that is found in the red-red zone the meniscus can, to some extent, heal and regenerate when damaged. The avascular region exhibits very poor self-repair capacity and tears situated in the white-white zone are more difficult to heal (Makris et al., 2011).

2.3 Osteoarthritis

Cartilage degradation can be the result of osteoarthritis, a joint disease that affects all joints in the body. The degradable events of OA are irreversible and often related to chronic pain. In severe cases, OA eventuates in complete cartilage loss that causes direct bone to bone contact (Arthritis Foundation, 2017). The knee joints are seemingly afflicted as they are complex joints that are vital for a functioning movement of the legs. Abrasive wear, as well as cartilage and meniscal lesions, are contributing factors to OA (Nguyen et al., 2017). Once a cartilage injury or meniscal tear has emerged, the degradable process is readily developed into OA.

OA is a joint disease that is the result of cartilage disintegration. Degradation of cartilage emerges in the event of impaired metabolism of ECM components (Gobbi & Lane, 2017, p. 6). Studies of OA-affected cartilage have indicated up-regulation of certain constituents of the ECM while components like the proteoglycan aggrecan

has reflected a decrease in its production (Maldonado & Nam, 2013). The imbalance in ECM synthesis introduces changes in the structural and biomechanical properties of cartilage. These differences constitute an altered environment for the chondrocytes that may trigger an inflammatory response that eventually worsens the OA advancement (Maldonado & Nam, 2013).

2.4 Aggrecan

The cartilage-specific proteoglycan core protein Aggrecan is a protein encoded by the ACAN gene. Aggrecan is the major proteoglycan in the articular cartilage. It is a carrier of chondroitin sulfate and keratan sulfate chains that enable the ability of articular cartilage to endure compressive loads (Roughley & Mort, 2014). Aggrecans are present in the ECM in the form of proteoglycan aggregates, where the aggrecan interact with hyaluronic acid (HA) through a link protein that preserves the interactions (Roughley & Mort, 2014). When synthetic and degradative events occur the structure of the chondroitin sulfate and keratan sulfate chains are transformed. Due to this degradation, cleavage is caused by all components of the aggregate (Roughley & Mort, 2014). A typical feature for native cartilage is the production of Collagen type II and aggrecan, these two characteristics are the underlying foundation of the extensive structural component of articular cartilage (Gatenholm, Lindahl, Brittberg, & Simonsson, 2020). Aggrecan has a function of being a chondrogenic marker as prechondrogenic characteristics are the results of the expression of aggrecans (Boreström et al., 2014).

The aggrecan contribution to the structure is not constituent during a whole existence, it is altered both due to synthetic and degradative events (Roughley & Mort, 2014). To boost the production of aggrecan thus inhibiting degradation, within the early stages of OA, the destructive process could be slowed down (Roughley & Mort, 2014). Tissue can not bear the rigors of joint loading without aggrecan (Roughley & Mort, 2014).

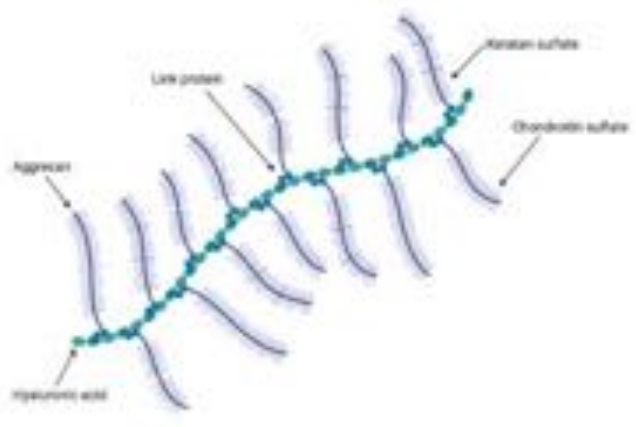

Figure 2.4: Several aggrecans attached to a backbone of hyaluronic acid. Bound to the aggrecans are keratan sulfate and chondroitin sulfate. Figure created with BioRender.com

There are properties required for a normal articular cartilage function (Roughley & Mort, 2014). Characteristics such as the capacity to form massive aggregates, having a high concentration of aggrecan, and an immense degree of aggrecan sulfation are such properties (Roughley & Mort, 2014). An equilibrium is required for the functional relationship of aggrecan in articular cartilage to contribute to an optimal cartilage function. The applied load on cartilage is balanced by the chondroitin sulfate and keratan sulfate chains' capability to swell when hydrated (Roughley & Mort, 2014). The proteoglycan aggregates containing chondroitin sulfate and keratan sulfate chains are enmeshed within collagen fibrils and the balance is obtained by the tensile forces that come with the stretching of the fibrils (Roughley & Mort, 2014). The resistance to load compression is primarily due to the high osmotic pressure of the charged chains (Huang & Wu, 2008). When the load on cartilage is removed the aggrecan have the ability to re-swell and obtain the balance between the swelling of aggrecan and the tensile forces induced by the stretching of collagen fibrils (Roughley & Mort, 2014). Aggrecan is involved in both the function of articular cartilage and the degradation of it in an OA affected joint. To limit aggrecan degradation and maintain aggrecan production can contribute to future treatments of early-stage OA (Roughley & Mort, 2014).

2.5 Induced Pluripotent Stem Cells

Embryonic stem (ES) cells are cells derived from the inner cell mass of a blastocyst. ES cells are characterized by their ability to form all three germ layers; ectoderm, endoderm, and mesoderm as well as their capability to grow indefinitely while remaining pluripotent. ES cells with their ability to differentiate into any cell type could potentially play an essential role in regenerative medicine (Boreström et al., 2014). The derivation of ES cells destroys an embryo at the blastocyst stage and to these cells is therefore strongly related to ethical concerns (Takahashi et al., 2007). Instead of utilizing embryos for the derivation of stem cells, pluripotency can be induced in already differentiated cells (Takahashi et al., 2007). These embryonic stem cell-like cells derived from somatic cells are not generating the same ethical considerations, hence they compose an alternative for future regenerative medicine.

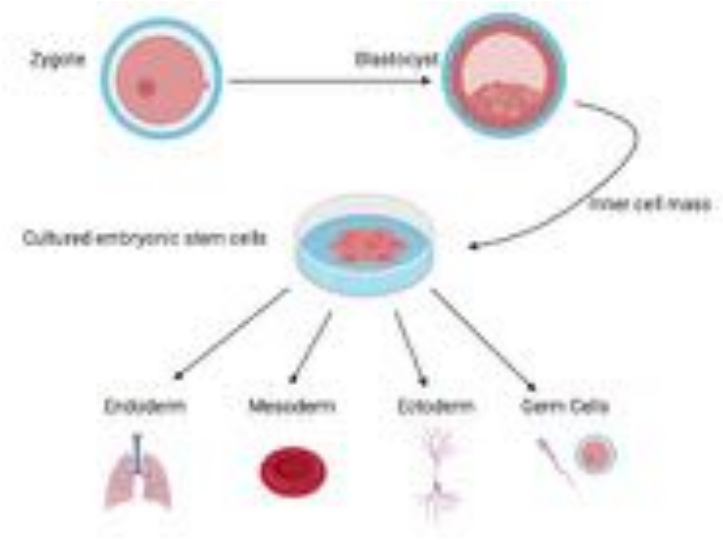

Figure 2.5: Embryonic stem cells can be derived from the inner cell mass of a blastocyst and cultured in vitro. Embryonic stem cells have the ability to differentiate into all three germ layers and germ cells. Figure created with BioRender.com

The induction of pluripotency into somatic cells by the introduction of four specific transcription factors, Oct3/4, Sox2, c-Myc, and Klf4 was first shown by Yamanaka in adult mouse fibroblasts in 2006 (Takahashi & Yamanaka, 2006). Further, the same approach was applied to human cells, and in 2007 induced pluripotent stem (iPS) cells from human fibroblasts were successfully achieved (Takahashi et al., 2007). The four transcription factors, also known as Yamanaka factors, are naturally expressed at high levels in ES cells and when introduced to somatic cells by retrovirus transduction, the differentiated cells become reprogrammed to iPS cells (Takahashi & Yamanaka, 2006). Verification of the in vitro produced iPS cells demonstrates similarities compared with ES cells regarding morphology, gene expression, and proliferation (Takahashi et al., 2007). Further attempts of inducing pluripotency to somatic cells have successfully been made with the use of other combinations of transcription factors. In 2007, human mesenchymal cells were reprogrammed with the transcription factors, OCT4, SOX2, NANOG, and LIN28 (Thomson et al., 1998).

With induction of pluripotency through viral transduction follows obstacles that need to be overcome before iPS cells can be applied in the clinic. With retroviral transduction, viral DNA is randomly integrated to the genome of the receiving cells (Medvedev, Shevchenko, & Zakian, 2010). Consequently, the integration of viral DNA is inconsistent and accounts for a great variation in the reprogramming process. Further, the transcription factors used for reprogramming might persist in iPS cells derived cells after differentiation. These transcription factors are highly related to tumorigenesis, hence the probability of tumor formation in iPS cells from retroviral transduction is high (Medvedev et al., 2010).

In order for iPS cells to be considered safe to use for clinical applications, reprogramming has to occur without the introduction of undesirable genomic alterations

(Boreström et al., 2014). In 2014, synthetic messenger RNA (mRNA) with genetic codes for OCT4, SOX2, KLF4, C-MYC, and LIN28 were successfully utilized for a footprint-free, non-invasive reprogramming of human somatic cells (Boreström et al., 2014). Reprogramming with mRNA accounts for less variation in expression of transcription factors compared with retroviral transduction since the mRNA quantity integrated into the cells can be controlled (Boreström et al., 2014).

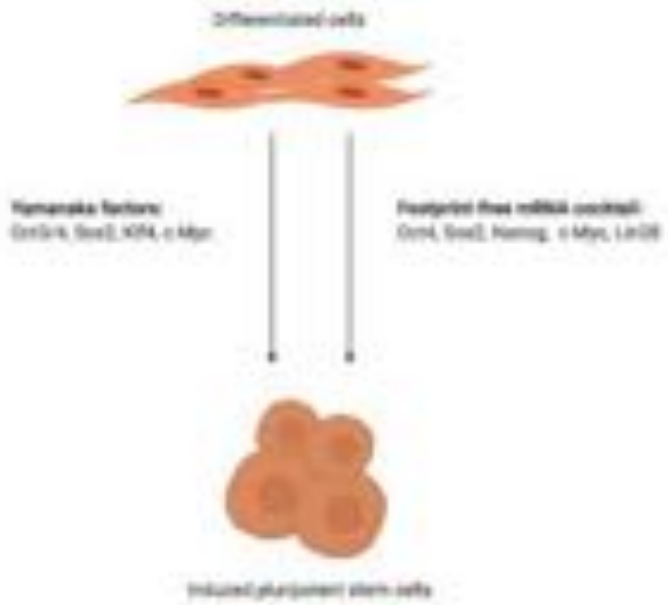

Figure 2.6: Two different approaches of reprogramming differentiated cells into induced pluripotent stem cells. Through viral transduction with Yamanaka factors and with a footprint-free mRNA cocktail. Figure created with BioRender.com

2.5.1 Differentiation into Chondrocytes

Induced pluripotent stem cells derived from chondrocytes can be re-differentiated into cartilage matrix-producing cells in vitro (Boreström et al., 2014). The remaining epigenetic memory is thought to be correlated to the ability of iPS cells to re-differentiate into the cellular origin with an aimed differentiation (Boreström et al., 2014). The differentiation time from pluripotent cells to chondrocytes includes three stages (Boreström et al., 2014). The chondrogenic progression, from a stem cell phenotype to a chondrogenic phenotype, involves the stages of primitive-streak mesendoderm to mesoderm intermediates to chondrocytes (Boreström et al., 2014). The differentiated iPS cells have shown to have an ability to reach the same expression levels as chondrocytes, before reprogramming, having the desired cartilage differentiation capacity (Boreström et al., 2014).

2.5.1.1 Medium with Additives for Chondrocyte Differentiation

In vitro differentiation can be established by the formation of 3D structures incubated at 37 ℃ and 5% CO_2 in a differentiation medium containing High-Glucose Dulbecco's Modified Eagle's Medium (DMEM) complemented with 1x ITS+, 100

nM Dexamethasone, 80 μM Ascorbic acid, 1 mg/ml Human serum albumin (HSA), 5 $\mu g/ml$ Linoleic acid, 1x penicillin/streptomycin (PEST), 10 ng/ml Transforming Growth Factor $\beta 1$ (TGF-$\beta 1$), 10 ng/ml Transforming Growth Factor $\beta 3$ (TGF-$\beta 3$), and 0,11 g/l Sodium pyruvate.

Cells cultured in a 3D environment contributes to differentiation as cells are permitted to grow and interact with their surroundings in all three dimensions, generating microtissues. A 3D aggregate formation with a defined number of iPS cells generates the opportunity to control the size of a shaped microtissue, and can be used for in vitro chondrogenic differentiation. According to Borestrom et al., 2014 mRNA-induced chondrocyte-derived iPS cells can differentiate to all three germ layers in vitro (Boreström et al., 2014). 3D cell cultures are more complex constructs than single-cell solutions as the cell-cell and cell-matrix interactions are dynamic. The differentiated iPS cells within the 3D constructs can correspond to in vivo tissues. A high cell density improves the communication between cells which is vital for chondrogenesis to occur (Boreström et al., 2014).

DMEM High-Glucose is DMEM modified with a raised glucose level to support primary cultures of cells and is suitable for both cell and tissue culture (Aldrich, 2020). Insulin-Transferrin-Selenium (ITS) is used as a basal medium supplement in order to boost the synthesis of nucleic acid and protein, intracellular transport, lipogenesis and to promote the amino acid and glucose uptake (Gibco, 2014). Transferrin serves as an iron carrier that the cell culture can benefit from as it may help to reduce toxic levels of peroxide and oxygen radicals (Gibco, 2014). Selenium is used as an antioxidant in the media (Gibco, 2014). Dexamethasone and TGF-$\beta 1$ are significant factors for the differentiation into chondrocytes (Enochson, Brittberg, & Lindahl, n.d.). One of the purposes of the addition of the L-ascorbic acid is to implicate the synthesis of collagen (Aldrich, 2020), and for the expansion of stem cells within tissue engineering, Human serum albumin is used (Aldrich, 2020). Linoleic acid, for use in cell culture, is typically bound to a carrier molecule such as HSA and increases the gene expression of its targeted genes (Aldrich, 2020). PEST is added to the medium as a supplement to maintain sterile conditions during cell culture by controlling bacterial contamination (Aldrich, 2020). With the addition of TGF-$\beta 3$ to the medium, the extracellular matrix production and chondrogenic gene expression are enhanced (Dahlin, Ni, Meretoja, Kasper, & Mikos, n.d.). To give the cells an approachable carbohydrate source, sodium pyruvate is added to the medium. The sodium pyruvate is also substantial since it is elaborated in Kreb's cycle and the amino acid metabolism (Aldrich, 2020).

2.6 3D Bioprinting

The technique of 3D bioprinting tissue and organs is emerging and possesses the potential of fundamentally changing the future of regenerative medicine (Nguyen et al., 2017). The course of action of 3D bioprinting resembles the procedure of the established 3D printing technique. Both methods utilize a layer-by-layer assembly of the ink but in 3D bioprinting, living cells are combined with bioink to generate

structures similar to real tissue. The ink intended for 3D bioprinting has to meet the biological demands and provide high cell viability as well as it has to display great printability (Markstedt et al., 2015).

Computer models derived directly from Magnetic Resonance Imaging (MRI) or Computerized Tomography (CT) scans enable personalized treatments where the bioprinted constructs can be made as a perfect fit of damaged tissue or as an exact replicate of an organ. Images from MRI or CT scans can be transferred to a Computer Aided Design (CAD) software to adjust the model properties (Semba, Mieloch, & Rybka, 2020). After the adjustments have been made in CAD, the file can be saved in Standard Tesselation Language (STL) and exported to a bioprinter where the final parameter settings before printing can be made (Semba et al., 2020). The result is a G-code ready to be printed into a patient specific tissue.

The technique behind 3D bioprinting varies and depends on the choice of bioprinter. The choice lies between the following three methods; inkjet, laser-assisted, and extrusion-based bioprinting. Inkjet bioprinting is similar to conventional inkjet printing. An inkjet bioprinter utilizes thermal or piezoelectric actuator methods to dispense the bioink in a contact-free manner in the form of small-scale droplets (Papaioannou et al., 2019). Thermal extrusion is a relatively cheap and widely used method where high temperatures can be generated in a short matter of time. The results are droplets of varying sizes but unfortunately cells and proteins are damaged due to the high temperatures (Li, Chen, Fan, & Zhou, 2016). Compared with thermal extrusion, piezoelectric technology is more gentle to the cells and proteins within the bioink and the droplets are more consistent in size (Li et al., 2016). Yet, piezoelectric actuator inquires bioinks with low viscosity which excludes some of the bioinks that are otherwise valid. Like inkjet bioprinting, laser-assisted bioprinting is also a contact-free method (Papaioannou et al., 2019). The technology behind laser-assisted bioprinting is to employ laser as an energy source that sends pulses onto a ribbon carrying bioink. The laser creates evaporation of the bioink that forms droplets on a receiving substrate (Li et al., 2016). The laser-assisted bioprinter prints without nozzles, hence no clogging in the nozzle tips occur and the cells are not exposed to stress due to pressure (Li et al., 2016). However, 3D bioprinting with a laser-assisted bioprinter may be a disadvantage to the cells because of it being a time consuming process. In extrusion-based bioprinting, pressure is applied to force the bioink through a nozzle onto a substrate. The pressure are either based on pneumatic (air) or mechanical forces (piston or screw) (Papaioannou et al., 2019). Extrusion-based bioprinting enables high cell densities, a uniform distribution of cells in the bioink, and the ability to print with a great extent of different biomaterials (Li et al., 2016). However, the method only allows for a great variation of bioinks if they fulfill the requirements of being viscous enough to avoid clogging in the nozzle tip and at the same time display a viscosity high enough to maintain the printed structure. Further, the bioink ought to shield the cells during printing and at the same time provide an environment favorable for the cells to thrive in.

Figure 2.7: An example of an extrusion-based bioprinter. The bioprinter in the figure is a Bio X™ from Cellink®. Adapted from (*BIO X - CELLINK*, 2020).

2.7 Nanofibrillated Cellulose and Alginate as Bioink

The bioink of a 3D bioprinted replica of a lesion that aims to develop into cartilage needs to be optimized within the parameters of viscosity, printability, fidelity, be noncytotoxic, withhold biocompatibility and obtain the environment that would promote the viability of cells. For a hydrogel bioink to be adequate for 3D bioprinting, there are specific characteristics of the bioink that need to be fulfilled. The requirement of a hydrogel as a bioink is a crosslinking qualification to acquire a shape fidelity of the 3D structure after printing (Markstedt et al., 2015). The printability of the hydrogel can be evaluated considering the parameters of the printer and the fidelity of the shape (Markstedt et al., 2015). Viscosity is an important characteristic if the viscosity decreases under shear strain the hydrogel has a shear thinning behavior. A challenge of bioprinting with a hydrogel is the tendency of a shape collapse because of low viscosity (Markstedt et al., 2015). The shear thinning property is desired while printing in combination with the crosslinking to prevent a shape collapse. According to Markstedt et al. (2015) a bioink that combines the outstanding shear thinning properties with the fast crosslinking ability is nanofibrillated cellulose (NFC) merged with alginate (A) (Markstedt et al., 2015). The combination of an NFC/A bioink together with cells was developed for the 3D bioprinting of living soft tissue with cells as it has been shown to present good cell viability (Markstedt et al., 2015).

A hydrogel has the ability to absorb and maintaining water without collapse and resembles the composition of articular cartilage as it is composed of 70-80% water (Semba et al., 2020). The naturally seaweed or bacteria produced polysaccharide alginate obtains the crosslinking ability as it is a linear polymer with a negative charge, thus resistance to dissolution as a result (Semba et al., 2020). The hydrogels of alginate are missing the capacity to bind cells and proteins on account of being negatively charged, however, alginates are non-toxic, non-immunogenic, biodegrad-

able, and biocompatible (Semba et al., 2020). To promote cell adhesion an addition of a positively charged biomaterial is needed (Semba et al., 2020). The negatively charged alginate enables an ionic crosslinking. The interacting cation determines the outcome regarding the hydrogel stability, mechanical properties and the hydrogel strength (Semba et al., 2020). The cation is shown most efficient to use when 3D bioprinting is calcium (Ca^{2+}) and a $CaCl_2$ solution results in a sufficient crosslinking agent (Semba et al., 2020). The 3D bioprinted constructs require a scaffold function, having a support and a stability quality. The result of adding NFC to the bioink contributes to mechanical support (Semba et al., 2020). The NFC and the alginate serve different purposes when acting as a bioink for 3D bioprinting. The alginate provides the resemblance of hyaluronic acid and proteoglycans meanwhile NFC resembles the bulk collagen matrix in cartilage (Nguyen et al., 2017). Alginate has shown to preserve iPS cells by encapsulation and plant-derived NFC enables the maintenance of iPS cell pluripotency. Both alginate and NFC have shown to maintain clustering into spheroids (Nguyen et al., 2017). Alginate and NFC are compliant to FDA and xeno-free materials (Nguyen et al., 2017).

The properties of NFC adds to shear thinning thus high shape fidelity before crosslinking and the properties of alginate dominate after crosslinking. The rheological characteristics as shear viscosity as well as the storage and loss modulus for the combination of NFC/A have shown the same viscosity flow curves similar to pure NFC, this indicates that crosslinking can be controlled by correlating to the alginate ratio without affecting the rheological properties (Markstedt et al., 2015).

Bioinks are being evaluated for potential involvement in treatments for cartilage defects and menisci injuries. The content of a developed bioink for 3D bioprinting can influence the phenotype of the developing tissue and the cell differentiation (Semba et al., 2020). The development and composition of a bioink is therefore a crucial step. The degradation products of bioink can not be toxic nor immunogenic (Semba et al., 2020). The biodegradation rate of the bioink needs to be with control hence corresponding to the cells' ECM remodeling capacity (Semba et al., 2020). The human body does not possess the ability to degrade alginate due to the absence of specific enzymes (Semba et al., 2020). According to Semba et al. (2019) only alginate polymers below the molecular weight of 48, 000 Da can be excreted by the urinary system (Semba et al., 2020). There are approaches to modify the alginate chains with chemical modifications to reach the molecular weight needed (Semba et al., 2020). Nanocellulose fibrils can be used to mimic cartilage as it is similar to collagen fibrils (Markstedt et al., 2015). The NFC based bioink in combination with alginate is noncytotoxic, biocompatible, and applicable in 3D bioprinting with living cells (Markstedt et al., 2015). As stated by Markstedt et al., 2015 alginate is compatible with cell culture and the cytotoxicity analysis of the bioink, containing NFC, resulted in no potential harmful effects as the cell viability was above 70% (Markstedt et al., 2015).

3

Methods

3.1 Cells and Cell Culture

Two different cell lines (A2B and H8) were cultured and used in the various experiments throughout the project period. Both cell lines originated from a 31-year-old female that donated surplus chondrocytes from autologous chondrocyte implantation (Boreström et al., 2014). The two cell lines had undergone reprogramming to become iPS cells with the use of Stemgent mRNA Reprogramming Kit. One of the two cell lines (H8) had been exposed to further modifications to express green fluorescent protein (GFP) under the aggrecan promotor. Prior to the ongoing project, the reprogramming into iPS cells and modification of one of the cell lines was performed at the Department of Clinical Chemistry and Transfusion Medicine, Institute of Biomedicine at Sahlgrenska Academy, University of Gothenburg. The cell lines were cryopreserved up until usage.

3.1.1 Cell Culture in a 2D Environment

Table 3.1: Medium, additives and reagents used for 2D cell culture.

Abbreviation	Product	Supplier
DEF-CS™	Cellartis® DEF-CS™ 500 Basal Medium with Additives	Takara BIO Europe AB
DPBS(-/-)	Gibco® Dulbecco's Phosphate Buffered Saline without Ca^{2+}/Mg^{2+}	ThermoFisher Scientific
DPBS(+/+)	Gibco® Dulbecco's Phosphate Buffered Saline with Ca^{2+}/Mg^{2+}	ThermoFisher Scientific
COAT-1	Cellartis® DEF-CS™ COAT-1	Takara BIO Europe AB
DMEM	Gibco® Dulbecco's Modified Eagle's Medium	ThermoFisher Scientific
TrypLE™	Gibco® TrypLE™ Select	ThermoFisher Scientific

The two cell lines were thawed and cultured in DEF-CS™ in a 2D-layer format. The cells were thawed in a water bath at 37 ℃, and centrifuged with DEF-CS™ at 700 *rpm* for 5 minutes. The cell pellet formed by centrifugation was dissolved in DEF-CS™ (0.2-0.3 ml/cm^2) with additives: GF1, GF2 and GF3. The cell suspension was transferred to a cell culture flask pre-treated with 0.1 ml/cm^2 of a 1:20 dilution of COAT-1 in DPBS(+/+) and incubated at 37 ℃ and 5% CO_2, medium change occurred every day. The cells were microscopically studied to be captured and passaged at confluency above 80%. When confluent, the cells were washed with DPBS(-/-) and exposed to enzymatic passage with 20 $\mu l/cm^2$ TrypLE™. Cells treated with TrypLE™ were incubated for 5 minutes and some gently tapping of the culture flask

occurred to aid the detachment of the cells from the surface. When all cells had separated from the culture flask surface, the enzymatic reaction was quenched by rinsing the surface with DEF-CS^{TM}. The cell suspension was transferred to a falcon tube and centrifuged at 700 *rpm* for 5 minutes to remove TrypLE^{TM}. After centrifugation the cells were counted with a Cell Counter (NucleoCounter® NC-200^{TM}, Chemometec) and seeded at a density of 30,000 cells/cm^2.

3.1.2 Cell Culture in a 3D Environment

With 2D cell culturing the objective is to provide a favorable environment for the iPS cells to proliferate but remain undifferentiated. When cultured in 3D, the aim is to allow the iPS cells to start differentiating and form cartilage tissue.

Table 3.2: Constituents mixed together to make pellet medium intended to be used in 3D cell culturing.

Abbreviation	Product	Supplier
DMEM	Gibco® Dulbecco's Modified Eagle Medium	ThermoFisher Scientific
PEST	Gibco® Penicillin-Streptomycin	ThermoFisher Scientific
ITS	Gibco® Insulin-Transferrin-Selenium	ThermoFisher Scientific
Ascorbic Acid		Apotekets productionunit, Umeå, Sweden
HSA/Linoleic Acid	Human Serum Albumin and Linoleic Acid	Sigma-Aldrich
Dexamethasone		Sigma-Aldrich
Sodium Pyruvate		Sigma-Aldrich
TGF-β1	Transforming Growth Factor	R&D systems
TGF-β3	Transforming Growth Factor	R&D systems

3.1.2.1 3D Culturing as Pellets

Cells from the established cell line A2B were cultured as pellets and supplemented with specific culture conditions to induce the differentiation of iPS cells into chondrocytes. Cells cultured in cell culture flasks were detached from the surface by the enzymatic reaction described in Section 3.1.1 to prepare a single-cell suspension. The detached cells were counted with the cell counter and transferred to a 96-well plate with the device INTEGRA Handheld Electronic 96 Channel Pipette VIAFLO 96 to reach a density of 200,000 cells per well with 125 μl medium per well. The 96-well plate was centrifuged at 700 *rpm* for 5 minutes and then incubated at 37 ℃ and 5% CO_2. Pellet medium prepared with the constituents stated in Table 3.2 was changed three times per week.

3.1.2.2 3D Culturing as Microtissues

Cells from both cell lines, A2B and H8, were cultured as microtissues. The microtissues were prepared in microwell culture plates (AggreWell^{TM} 800, STEMCELL Technologies) where each plate consisted of 24 wells with 300 microwells per well. The wells were pre-treated with Anti-Adherence Rinsing Solution to avoid extensive cell adherence. Anti-Adherence Rinsing Solution (STEMCELL Technologies) was added to each well and the plate was centrifuged at 3200 *rpm* for 5 minutes. The Anti-Adherence Rinsing Solution was discarded and each well was washed with warm pellet medium. A single-cell suspension was prepared as described in Section

3.1.2.1. The cells in the single-cell suspension was counted in the cell counter and distributed to reach a cell density of 10,000 cells/microwell and 3×10^6 cells/well. The cell suspension was pipetted up and down in each well to allocate the cells evenly in each microwell. The plate was centrifuged at 1500 *rpm* for 3 minutes and then left to incubate for 3 days at 37 ℃ and 5% CO_2.

The microtissues were harvested after 3 days of incubation. For harvesting of microtissues, medium was gently flushed in the wells to free the microtissues from the microwells. The plates were continuously studied under a microscope to ensure that all microtissues were dislodged and the flushing was repeated until all wells were empty. The microtissues were transferred to well plates and incubated with shake (30 *rpm*) until further usage.

3.2 Optimization of Bioink

Three different ratios of nanofribrillated cellulose and alginate (NFC/A) were analyzed and compared in the optimization of bioink. The nanofibrillated cellulose source was cellulose fibers (Sigma-Aldrich) from cotton linters and the cellulose was mixed in a grinder to achieve fibers of smaller sizes. The dimensions of the fibers were not measured after the mixing process but were expected to be of nano-size. The alginate used was sodium alginate (Sigma-Aldrich) derived from brown algae. The dry weight of alginate per total liquid volume (w/v) was uniform in all three bioink compositions; 48/52, 60/40, and 80/20 NFC/A (% w/w). The alginate was kept constant since the selected concentration had previously indicated to be favorable for the cells during and after bioprinting. The dry weight of NFC, however, was varied to enable the investigation and optimization of the three different bioink compositions. Table 3.3 displays the final w/v concentration of both NFC and A in the three different bioinks.

Table 3.3: Three different bioink compositions exposed to analysis and the weight per volume concentration of nanofibrillated cellulose and alginate in each bioink respectively. The volume (v) refers to the total liquid volume including WFI, DMEM and $CaCl_2$.

NFC/A (w/w)	NFC (w/v)	A (w/v)
48/52	5.6	5.9
60/40	8.9	5.9
80/20	29.5	5.9

In the initial stages of the optimization, all three bioinks were prepared in a non-sterile environment. The non-sterile preparation of the bioinks was performed to

comprehend the protocol and to provide a fundamental understanding of the procedure. To be able to introduce cells to the bioinks, the same protocol was conducted with aseptic techniques. Before the production, all constituents were autoclaved to ensure sterile conditions. After sterilization, the components were combined by first mixing alginate with Water For Injection (WFI) for Cell Culture (Gibco^{TM}, ThermoFisher Scientific), adding NFC and DMEM to the alginate-water mixture and lastly crosslink the alginate with 90 mM $CaCl_2$ under constant stirring. The completed bioink was stored at 4-6°C up until analysis. Properties such as fidelity, stability, viscosity, and shear thinning are important for proper 3D-bioprinting of tissues. These parameters were therefore thoroughly investigated in the optimization of bioink.

3.2.1 Sterilization of Bioink Components

To ensure the elimination of microorganisms and their spores, it was of great importance that all bioink components were subjected to sterilization before bioprinting. The sterilization process applied in the optimization of bioink was to autoclave the NFC and alginate before the constituents were mixed. Both NFC and alginate were pre-weighed and put in eppendorf tubes in autoclavable bags and the sterilization was carried out at 121-134 ℃. An additional of 4-8 % of alginate powder was added in the pre-weighing to account for losses during the autoclave process.

3.2.2 Printability Test

The printability of the bioink ratios 48/52, 60/40 and 80/20 NFC/A *(% w/w)* was evaluated by diameter measurements of the 3D printed constructs. The three bioink ratios were obtained by keeping the alginate concentration constant with the varying concentration of NFC, as described in Section 3.2. The viscosity of a hydrogel contributes to the level of the viability of cells. A hydrogel with a low viscosity has higher cell viability, resulting in a low printing fidelity and stability. The focus of the optimization of the bioink therefore lies within reaching the balance between cell viability and printing accuracy.

A 10×10 mm square was 3D printed with each bioink ratio and three replicates were obtained respectively, see Figure 3.1. After one layer of the structure had been printed the measurements of both the diameter and the length of the corner were obtained. The nine squares were 3D printed with a speed of 4 mm/s and the pressure of 15 kPa.

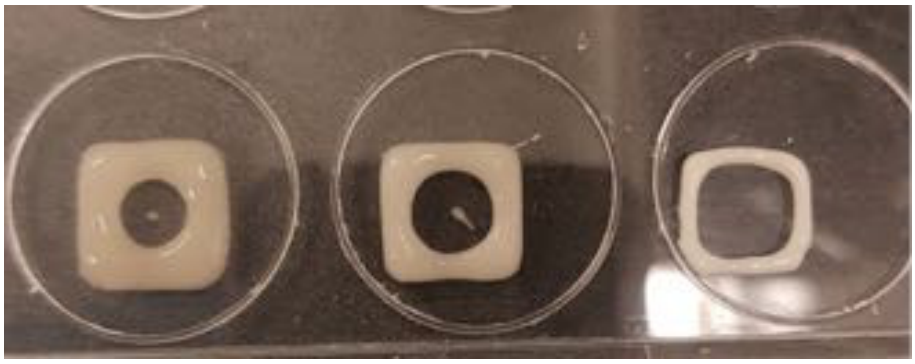

Figure 3.1: A printability test of the bioink ratios 48/52, 60/40 and 80/20 NFC/A (*% w/w*).

Further, the bioinks were 3D printed as S-shapes to evaluate the printability of more complex shapes. Two replicates of each bioink were printed as an S of 1 *cm* in height and in 3 layers, see Figure 3.2. The 3D printed constructs were immediately crosslinked with 100 mM $CaCl_2$ before the shape fidelity and stability were studied.

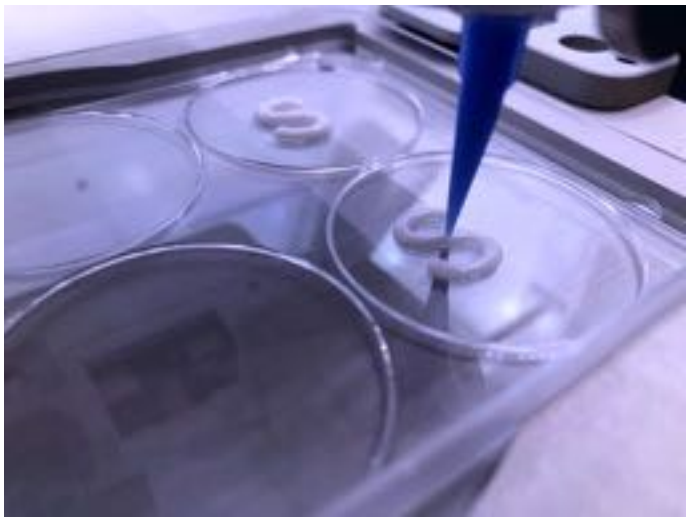

Figure 3.2: 3D printed S-shapes of 1 *cm* in height and in 3 layers.

3.2.3 Rheology

Measured rheological properties of a bioink provide an insight into how the bioink will perform when 3D printed. A bioink that is printable with a low pressure is desired since low pressure will promote the cell viability when 3D bioprinting with living cells

Viscosity ($Pa \times s$) versus shear rate (s^{-1}) were measured with a Discovery Hybrid Rheometer 3 (HR-3), TA Instruments UK, with the geometry Peltier 40 mm parallel plate in steel. The procedure selected was a shear sweep with a flow ramp at 25°C and 600,0 s. The rheological properties of seven different bioinks were analyzed, see Table 3.4.

Table 3.4: The 7 different bioinks prepared and analyzed for their rheological properties.

Number	Bioink	NFC	Alginate
1	48/52 NFC/A	Autoclaved NFC	Autoclaved sodium alginate
2	60/40 NFC/A	Autoclaved NFC	Autoclaved sodium alginate
3	80/20 NFC/A	Autoclaved NFC	Autoclaved sodium alginate
4	Alginate	-	Autoclaved sodium alginate
5	Alginate	-	Sodium alginate
6	60/40 NFC/A	Autoclaved NFC	PRONOVA^{TM} SLG100
7	60/40 NFC/A	CELLINK LAMININK 521	PRONOVA^{TM} SLG100

All of the seven different bioinks contained alginate, either SIGMA-ALDRICH sodium alginate or PRONOVA^{TM} SLG100. The type of alginate used in each bioink is specified in Table 3.4. The ratios 48/52, 60/40 and 80/20 NFC/A (*% w/w*) (number 1-3 in Table 3.4) where both NFC and sodium alginate had been autoclaved were evaluated. Pure sodium alginate, both autoclaved and not autoclaved (number 4-5 in Table 3.4), mixed as bioinks were examined. These bioinks with pure sodium alginate were produced as the NFC/A bioinks; containing DMEM, WFI, and crosslinked with 90 mM $CaCl_2$, the only difference was the absence of NFC. The rheological properties of the bioink used for 3D bioprinting of small-scaled meniscus (number 6 in Table 3.4), see Section 3.4, and the bioink used for 3D bioprinting for transplantation (number 7 in Table 3.4), see Section 3.5, were also measured. The bioink for the 3D bioprinted small scale menisci and the bioink for the transplantation both contained a 60/40 ratio NFC/A (*% w/w*). The small scale menisci consisted of 40% w/w of the sterile alginate PRONOVA^{TM} SLG100 combined with 60% w/w autoclaved NFC. The bioink for the transplantation was composed of CELLINK LAMININK 521 diluted with the sterile alginate PRONOVA^{TM} SLG100 to achieve the desired bioink ratio.

3.3 Viability Tests

The cell viability in the various bioinks was evaluated to find the optimal ratio NFC/A (*% w/w*). A variety of approaches as well as the use of both 2D and 3D cell culturing to measure the cell viability were carried out and are described in the following sections. The viability of cells was analyzed by the calculation of living cells in the different bioink ratios. One approach was to count live and/or dead cells with the cell counter, another technique used was to count cells with the Bürker Chamber method. Viable cells within 3D bioprinted constructs were counted with LIVE/DEAD® viability assay and images were obtained with confocal microscopy.

The Bürker Chamber consists of a glass plate with two fields that are separated. The two chambers have 9 large 1 mm^2 fields marked with three parallel lines and are each divided into 16 smaller squares. The viability was determined by the number of viable cells per ml. The average cell count from each of the sets of the 16 squares was therefore taken. Every large square has a depth of 0,1 mm hence a volume of

10^{-4} mL and the concentration of cells can be calculated, see Equation 3.1.

$$C = N \times S \times 10^4 \tag{3.1}$$

The number of cells per ml can be estimated where C is the cell concentration, N is the number of cells per 1 mm^2 and S is the dilution of the cell suspension.

3.3.1 Cell Viability - Monolayer

An initial evaluation of the cell viability in the three different bioinks was performed with cells cultured in monolayers and covered with bioink, see Figure 3.3. Two 6-well plates were pre-treated with 0.1 ml/cm^2 of a 1:20 dilution of COAT-1 in DPBS(+/+) before cells from the established cell line A2B were seeded in the wells. The cells were seeded with a density of 100,000 cells/well and incubated at 37 ℃ and 5% CO_2 for 4 days with medium (DEF-CS^{TM} with additives) change every day. After 4 days, 48/52, 60/40 and 80/20 NFC/A (% w/w) bioinks were added to the wells with 3 replicates of each bioink as well as 3 controls without bioink. The bioink was dispersed with a 5 ml syringe, 2 ml bioink in each well to achieve full coverage of all cells. To crosslink, 1 ml of 100 mM $CaCl_2$ was added to each well. After 5 minutes, the $CaCl_2$ was removed and 1 ml medium (DEF-CS^{TM} with additives) was added to the wells. The plates were incubated for 24 hours in 37 ℃ and 5% CO_2.

After 24 hours of incubation, the bioink was removed with a spatula. The cells were enzymatically detached from the well plates with TrypLE^{TM} as described in Section 3.1 and counted with the cell counter.

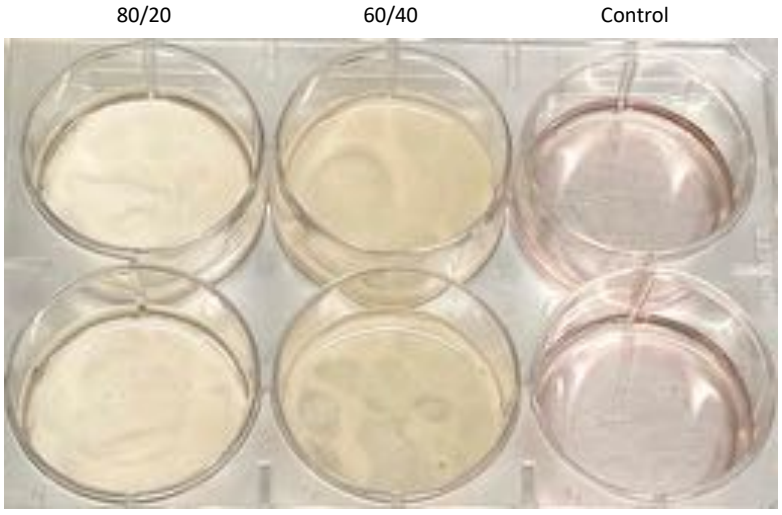

Figure 3.3: 2D cultured iPS cell monolayer covered with 80/20 and 60/40 NFC/A (% w/w) bioink together with two controls without bioink.

3.3.2 Cell Viability - Pellets

Cells from the established cell line A2B were cultured in cell culture flasks and when confluent, a fraction of the cells were collected and transferred to a 3D environment

allowing them to form pellets. The procedure for 3D culturing as pellets is described in Section 3.1.2.1. A 96-well plate composed the 3D environment for the pellets, one pellet/well, where each pellet comprised approximately 200,000 cells. After 2 weeks of 3D culturing the cell pellets were exposed to a 200 μl layer of bioink directly in the 96-well plate. It was desired to evaluate the viability of the cells after the pellets had been exposed to the bioink for 1 week. The 3 different bioink ratios analyzed were 48/52, 60/40 and 80/20 NFC/A (% w/w). Each bioink generated 3 replicates respectively and 3 pellets without bioink were used as controls, see Figure 3.4. After the bioink was applied, $CaCl_2$ was added for 5 minutes to crosslink the bioink. Before incubation in 37°C and 5% CO_2, 50 μl pellet medium was added to all wells containing both pellet and bioinks. Meanwhile, 100 μl pellet medium was added to the 3 controls.

A Collagenase II-treatment was prepared one week after the pellets had been exposed to bioink. The purpose of the Collagenase II-treatment was to separate the cells in the pellets and obtain a single cell solution before counting the cells. The bioink was dissolved in DPBS(-/-) and then removed. The pellets were washed with DPBS(+/+) and incubated in 37℃ and 5% CO_2 overnight with a 8 mg/ml Collagenase II/F-12 (Gibco Ham's F-12 Nutrient Mixture, ThermoFisher Scientific) treatment. The 3 replicates of each sample were pooled in a centrifuge tube with F-12 and centrifuged at 1,300 rpm for 5 minutes. The supernatant was discarded and centrifuged with F-12 once more at the same rate. The pellets were dissolved in pellet medium and counted manually with the Bürker chamber method under a microscope.

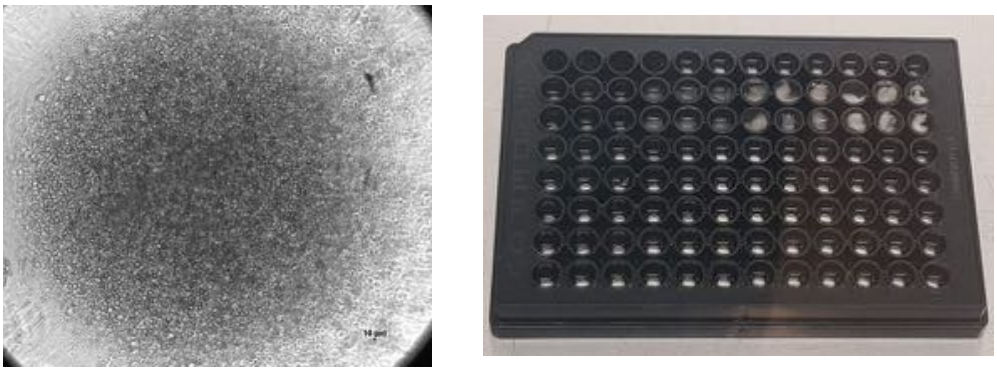

Figure 3.4: Image of one iPS cell pellet to the left and 3D cultured microtissues covered with 48/52, 60/40 and 80/20 NFC/A (% w/w) bioink together with controls without bioink.

3.3.3 Cell Viability - Cells in Bioink

A viability test to evaluate single-cell suspensions in a 3D environment with bioink were obtained to further provide data to the optimization of bioink. The bioinks used were acquired through aseptic technique and the bioink ratios evaluated were 48/52, 60/40, and 80/20 NFC/A (% w/w). The amount of cells used in total was

counted to 4,33× 10^6 cells with the cell counter. The cell suspension had a volume of 1 ml which was divided equally over the three bioink samples and further divided evenly over five replicates respectively, hence approximately 289,000 cells per replicate. Each bioink sample containing 333 μl cell suspension together with 667 μl bioink (1:3 cells:bioink) was mixed by attaching the bioink syringe to the syringe with cell suspension with a female/female luer lock adaptor. A 48-well plate was used for the evaluation and the samples were divided into each well with the syringe now containing the mixture of the bioink and the cells in suspension, see Figure 3.5. All replicates contained a total volume of 200 μl of the samples, 50 μl of $CaCl_2$ solution as a crosslinker that was discarded after 5 minutes and 250 μl medium (DEF-CS$^{\text{TM}}$ with additives) in each well.

The viability of the cells in the single-cell suspensions dispersed in bioink was evaluated after incubation for 8 days. The viability for the three different NFC/A bioink ratios were determined with Bürker Chamber. The five samples for each bioink ratio were pooled together in a 15 ml Falcon Tube respectively since the division into five exact volumes of bioink and the cell suspension was not successful. The cell medium was discarded and the samples were treated with DPBS(-/-) to dissolve the bioink. After the DPBS(-/-) treatment the three 15 ml Falcon Tubes were centrifuged at 1500 rpm for 5 min, the DPBS(-/-) was discarded and 10 μl of each sample were added to a Bürker Chamber. The number of cells counted with Bürker Chamber corresponded to the value of N in Equation 3.1 and the cell viability could be calculated.

Figure 3.5: Five replicates of single iPS cell solution mixed with 48/52, 60/40 and 80/20 NFC/A (% w/w) bioink respectively.

3.3.4 Cell Viability - Bioprint

Cells from the established cell line A2B were cultured in microwell culture plates as described in Section 3.1.2.2 to induce the formation of microtissues. The A2B cell

line was cultured in a microwell culture plate for three days. After harvesting, the microtissues were kept in pellet medium and transferred to a 1 ml syringe and attached to another 1 ml syringe containing bioink with a female/female luer lock adaptor. The microtissue-suspension was carefully mixed with the bioink through a female/female luer lock adaptor. The mixing resulted in a 1:10 microtissue-suspension:bioink-solution.

The bioink ratios evaluated were 60/40 and 80/20 NFC/A *(% w/w)*. As the number of microtissues in each well slightly differed, the concentration of cells for the 60/40 NFC/A *(% w/w)* bioink was 16,32× 10^6 cells/ml and 17,2× 10^6 cells/ml for 80/20 NFC/A *(% w/w)*. The bioinks utilized were produced with aseptic technique containing autoclaved NFC, autoclaved alginate, WFI, DMEM with the supplement PEST and crosslinked with 90 mM $CaCl_2$ solution. Approximately 500 µl was printed for each bioink ratio containing approximately 20×10^6 cells/ml.

A 3 mm small droplet was 3D bioprinted with BIO X™ (Cellink®) bioprinter with a 22G - 410 μm nozzle, at 4 mm/s and with the pressure 15 KPa, see Figure 3.6. Two 6-well plates were used for each bioink ratio resulting in 12 replicates per sample, thus approximately 700,000 cells/replicate (70 microtissues/droplet). The two bioink samples with 6 replicates respectively were all crosslinked with a 100 mM $CaCl_2$ solution for 5 minutes, before the addition of 2ml PM and the incubation in 37°C and 5% CO_2.

The cell viability was evaluated by a LIVE/DEAD® viability assay and analyzed in Nikon® confocal microscope (A1 HD25/A1R HD25) utilizing the settings Alexa Fluor® 488 and Alexa Fluor® 546 for the Calcein AM and the Ethidium homodimer-1 dyes. Three replicates of each of the two different bioinks as well as a dead control, all 3D bioprinted as 3 mm droplets containing microtissues, were studied after 1 week, 4 weeks, and 5 weeks in the confocal microscope.

Figure 3.6: Microtissues harvested, immersed in bioink and 3D bioprinted as small 3 mm droplets with the BIO X™ (Cellink®).

3.3.4.1 Live/Dead Staining

LIVE/DEAD® Viability/Cytotoxicity Kit (ThermoFisher Scientific) was utilized to perform a viability assay of constructs printed with 60/40 and 80/20 NFC/A *(% w/w)* as described in Section 3.3.4. Two different dyes were combined to be able to distinguish between live and dead cells; Calcein AM, a cell-permeable dye that exhibits green fluorescence in live cells and Ethidium homodimer-1 (EthD-1), that is not cell-permeant and thereby contributes to red fluorescence in dead cells.

The two dyes were stored in the freezer up until usage and allowed to thaw at room temperature. First, 2 mM EthD-1 was added to DPBS(+/+) to reach a final 4 μM EthD-1 solution. The two components were mixed by vortexing. Second, 4 mM Calcein AM in Dimethyl sulfoxide (DMSO) was added to the 4 μM EthD-1 solution to achieve 2 μM Calcein AM. Vortexing was once again carried out to ensure a complete mixture of the two dyes.

Bioprinted constructs were transferred to microcentrifuge tubes. Three replicates of each print (60/40 and 80/20) were prepared for each measurement. The prints were washed with DPBS(+/+) and covered with the dye solution and incubated at 37 ℃ and 5% CO_2 for 50 minutes. A dead control was also prepared by covering a print with 75% ethanol and incubate in a freezer for 20 minutes before the construct was covered with dye solution. LIVE/DEAD® viability assay was performed 1, 4, and 5 weeks after bioprinting. A drop of DAPI was added to the samples analyzed 5 weeks after bioprinting to get a hint of the cell nuclei in the bioprinted constructs.

After 50 minutes incubation time the prints were transferred to 25× 75× 1 mm microscope slides $SuperFrost^*/Plus$ (MENZEL-GLÄSER®) and covered with 24×60 mm cover slips Deckgläser (MENZEL-GLÄSER®) and studied in confocal microscope, utilizing the settings Alexa Fluor® 488 and Alexa Fluor® 546 for the Calcein AM and the Ethidium homodimer-1 dyes.

3.4 3D Bioprinting Meniscus

3D cultured microtissues combined with bioink are used in 3D bioprinting of living tissues and organs. The number of cells per ml bioink needs to be optimized for tissue generation as parameters such as viability, contact, and nutrient availability need to be balanced. The 3D bioprinting of small-scaled meniscus was implemented with the optimized bioink 60/40 NFC/A (% *w/w*). The evaluation was performed with autoclaved NFC and PRONOVA™ SLG100 alginate.

The 3D bioprinting of menisci was executed with 3D cultured microtissues harvested as described in Section 3.1.2.2. The cell line utilized was A2B cultured microtissues. The 60/40 NFC/A (% *w/w*) bioink utilized was produced with aseptic technique containing autoclaved NFC, PRONOVA™ SLG100 alginate, WFI, DMEM with the supplement PEST and crosslinked with 90 mM $CaCl_2$ solution. Approximately 600 µl was printed containing $10{\times}10^6$ cells/ml, hence 100 microtissues/ml. As the

bioink had a non-printable viscosity, the bioink was diluted with a total of 1 ml DMEM to contribute to the possibility of 3D bioprinting with cells. The small scale menisci of 3 mm were 3D bioprinted with a speed of 3-4 mm/s, with the pressure 20-30 kPa and with a 22G nozzle. One control containing nothing but bioink, and five replicates of 60/40 NFC/A ($\%$ w/w) including cell suspension, were obtained and printed in a 6-well plate. The control was printed with 3 mm/s at 75 kPa. The 3D bioprints were crosslinked with a 100 mM $CaCl_2$ solution for 5 minutes before the addition of 2 ml medium (PM) and incubation in 37°C and 5% CO_2. A 3D printed full-scale meniscus printed without cells can be seen in Figure 3.7.

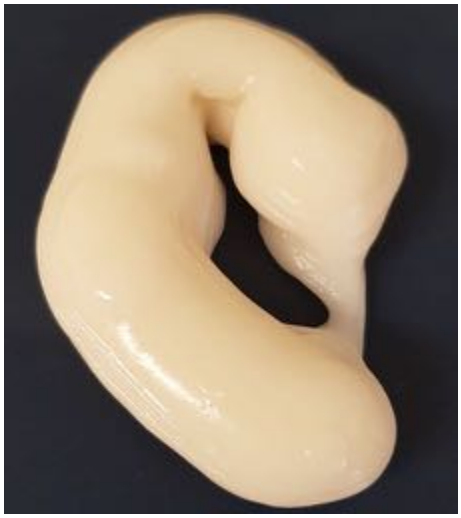

Figure 3.7: A 60/40 NFC/A (w/w) bioink 3D printed full scale medial meniscus, printed without cells.

3.4.1 Evaluation of 3D Bioprinted Meniscus

For evaluation, two of the 3D bioprinted menisci were immersed in a 100 mM $CaCl_2$ solution one month after 3D bioprinting. Thus the constructs were prevented from collapse, before the immerse in Histofix Fixation Solution to maintain tissue structure. The samples were sent to Histolab Products AB for embedding, sectioning, and staining with Alcian Blue van Gieson. The paraffin-embedded tissues were analyzed with digital imaging with Nikon® Instruments' Eclipse 90i.

Immunohistochemical staining was implemented to analyze the microtissues within the 3D bioprinted small-scale menisci. Evaluation of 3D bioprinted menisci were accomplished by deparaffinization of the paraffin-embedded tissue slides as incomplete removal of paraffin can consequently yield poor staining. The materials and reagents used for the deparaffinization of the slides were Xylene, 99% ethanol, 95% ethanol, 70% ethanol, and PBS. An antigen retrieval step was conducted with 10 mM citrate buffer pH 6.0 and hyaluronidase 8000 $units/ml$ was introduced for digestion. A blocking step with 10% goat serum in 1×PBS was implemented to block unspecific binding sites before introducing the samples to the primary antibody anti-human collagen type II mouse with a dilution 1:400 in 10% goat serum in 1×PBS. After

rinsing and another blocking step with 10% goat serum in 1×PBS, the sections could be stained with secondary antibody goat anti-mouse Alexa 546 with dilution 1:300 in 10% goat serum in 1×PBS. The sections were rinsed and stained with ProLong® Gold antifade reagent with DAPI to be studied in confocal microscope. A positive and a negative control containing chondrocytes underwent the same protocol, the negative control with the neglect of primary antibody. The stained sections were studied with fluorescence microscopy with Alexa Fluor® 546.

The cell viability of the 3D bioprinting of small-scaled menisci was analyzed by a LIVE/DEAD® viability assay and evaluated in a confocal microscope, see Section 3.3.4.1.

3.5 3D Bioprinting for Transplantation

Two transplantation studies with 3D bioprints were acquired. With a future aim to be able to remotely control, stimulate, and monitor cartilage repair, evaluation of the high electrical conductivity additive carbon nanotubes (CNTs) was obtained. This analysis also included a study of a non-steroidal anti-inflammatory drug, loaded or unloaded within the samples. The first trial was carried out with bioink in combination with the iPS cell line A2B harvested as microtissues and cultured for three weeks. The 3D prints were printed as droplets on COPLA Scaffolds™ - medical devices for cartilage repair (Askel Healthcare). The cells were 3D cultured as described in Section 3.1.2.2, seeded on the COPLA Scaffolds™ and the bioink was 3D printed, with BIO X™(Cellink®) at 140 KPa with 5 s per droplet, covering the microtissues. The ratio cell suspension/bioink used was 1:10 which resulted in approximately $20{\times}10^6$ cells/ml.

The second trial was implemented with crosslinked nanoemulsions unloaded or loaded with an anti-metastatic drug, both loaded with Nile RED. The cells were 3D cultured as described in Section 3.1.2.2 and the iPS cell line used was the modified H8 harvested as microtissues and cultured for one month. The microtissues were immersed in bioink and 3D bioprinted with BIO X™(Cellink®) with the droplet function at 60 KPa with 5 s per droplet. The ratio cell suspension/bioink used was 3:10 which resulted in approximately $20{\times}10^6$ cells/ml.

The bioink for the two transplantation studies was produced using CELLINK LAMININK 521 diluted with PRONOVA™ SLG100 to reach the optimized percentage of 5.9% alginate used within this project. The bioink was prepared with PRONOVA™ SLG100, WFI, DMEM with the supplement PEST, and CELLINK LAMININK 521 crosslinked with 90 mM $CaCl_2$. The bioink was produced with an aseptic technique in the written order.

For the first trial, 36 implants were surgically transplanted in 18 mice. For the second trial, 20 implants were surgically transplanted in 10 mice. Both trials were performed by surgeons at Sahlgrenska Academy and implemented according to a procedure that was approved by the Ethical Committee in Gothenburg. The im-

plants were *in vivo* cultured in mice for 5 weeks before they were explanted and analyzed

To examine the 3D bioprinted constructs for transplantation, the remaining constructs that were not transplanted were immersed in a 100 mM $CaCl_2$ solution before they were immersed in Histofix Fixation Solution to maintain their tissue structure. The samples examined were one 3D bioprinted construct consisting of bioink and cell suspension, one construct unloaded and one construct loaded with the anti-metastatic drug. The samples were sent to Histolab Products AB for embedding, sectioning and staining with Alcian Blue van Gieson. The paraffin-embedded tissues were analyzed with digital imaging with Nikon® Instruments' Eclipse 90i.

Immunohistochemical staining was implemented to analyze the microtissues within the 3D bioprinted constructs. An evaluation of the constructs was accomplished by deparaffinization of the paraffin-embedded tissue slides, see Section 3.4.1. To be able to evaluate the sections for transplantation a positive and a negative control containing chondrocytes underwent the same protocol, the negative control with the neglect of primary antibody. The stained sections were studied with fluorescence microscopy with Alexa Fluor® 546.

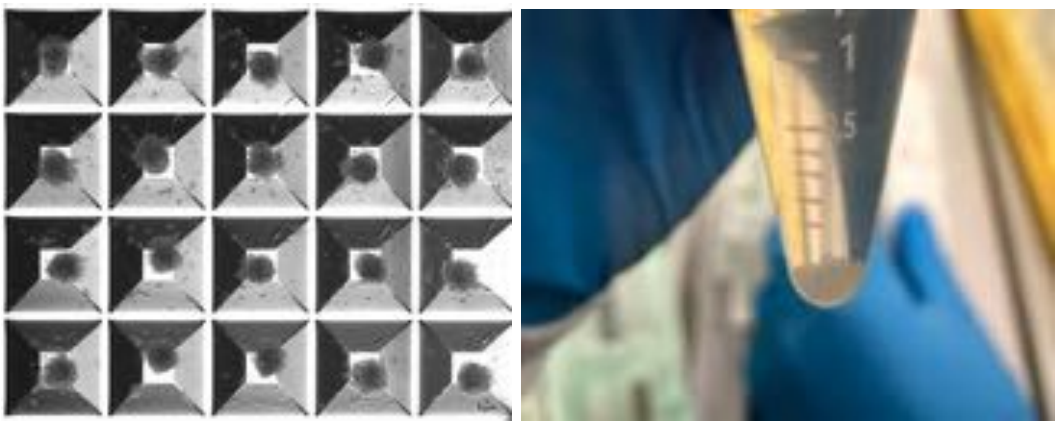

Figure 3.8: 3D culturing of microtissues in a microwell culture plate to the left and harvested microtissues prior to 3D bioprinting to the right.

3.6 Differentiation of iPS cells in 3D cell culturing

Microtissues, 3D cultured as described in Section 3.1.2.2 were utilized in the 3D bioprinted constructs when 3D bioprinting both menisci and the transplantation constructs. The microtissues were dispersed in bioink and 3D bioprinted to enable a scaffold with 3D environment, thus implementing a differentiation capacity of the iPS cells to chondrocytes. Some microtissues that were not utilized in any of the bioprinting processes were cultured and subjected to further evaluations.

3.6.1 Morphology

To evaluate the morphology of the differentiated iPS cells approximately 150 microtissues cultured for two months were pooled together. The microtissues were washed with PBS +/+ and treated with a collagenase digestion cocktail, which contained 8 mg/ml collagenase II/F-12, and incubated in 37°C and 5% CO_2 overnight. The cell suspension was washed with 10 ml F-12 at 1300 rpm two times before the resulting single cells were seeded in a coated 25 ml culture flask with a chondrocyte medium consisting of Dulbecco's Modified Eagle Medium: Nutrient Mixture F-12 (DMEM/F12), PEST, Human serum, and ascorbic acid. The cultured cells were observed with Nikon® Eclipse Ti Series, combined with Nikon's NIS-Elements imaging software.

3.6.2 Immunohistology

One of the two-month cultured microtissues was immersed in Histofix Fixation Solution to maintain the tissue structure, and stored in 70% ethanol. The sample was sent to Histolab Products AB for staining with Alcian Blue van Gieson. The paraffin-embedded microtissue was analyzed with digital imaging with Nikon® Instruments' Eclipse 90i. Immunohistochemical staining was implemented to further analyze the microtissue. An evaluation of the microtissue was accomplished by deparaffinization of the paraffin-embedded sections, following the same protocol as conducted in Section 3.4.1. The microtissue was stained for collagen type II. To be able to evaluate the microtissue, a positive control containing chondrocytes underwent the same protocol. The stained sections were studied with confocal microscopy with Alexa Fluor® 546.

3.6.3 Real-Time Quantitative Reverse Transcription-PCR

Quantitative Reverse-Transcription Polymerase Chain Reaction (qRT-PCR) is a method to quantify the gene expression of the cells. Cells from the established cell line A2B that had been cultured as microtissues for 3 months were exposed to qRT-PCR to verify if the cells expressed RNA-sequences typical for stem cells or for differentiated cells. Two samples were prepared, each containing ∼20-30 microtissues. The medium was removed and the dry microtissues were kept in liquid nitrogen. The RNA isolation from the microtissues was performed with TissueLyser LT, Qiazol and Qiagens RNeasy Micro Kit (Qiagen), a method from RNeasy® Lipid Tissue Mini Kit. The microtissues were shaken 2 × 2 minutes at 50 Hz in a TissueLyser LT (Qiagen) with two 5 mm bullets per sample. Quiazol was added and the tubes were once again shaken for 2 × 2 minutes at 50 Hz. For the purification of RNA, 1-Bromo-3-chloropropane (BCP) was added and the samples were centrifuged at 13,000 rpm for 15 minutes. The supernatant was collected, mixed with 70% ethanol, and transferred to MinElute (micro) spin columns (Qiagen). Buffer RW1 (Qiagen), DNase mix (DNase and buffer RDD, Qiagen), buffer RPE (Qiagen), and 80% ethanol were added sequentially for washing membrane-bound RNA. Finally, the samples were eluated with H_2O before the concentrations were measured.

For the reverse transcription reaction, where RNA is synthesized into complementary DNA (cDNA), the High-Capacity cDNA Reverse Transcription Kit (Applied Biosystems^{TM}, ThermoFisher Scientific) was combined to form a Master Mix. The Master Mix contained H_2O, 10× RT Buffer, 10× RT Random Primers, 25× dNTP Mix, MultiScribe^{TM} Reverse Transcriptase, and RNase Inhibitor. The RNA concentrations in the two samples were diluted in H_2O and mixed with the Master Mix to reach a final concentration of 35 $ng/\mu l$ RNA prior to the cDNA synthesis. The cDNA synthesis was carried out at 25℃ for 10 minutes, at 37℃ for 120 minutes, and finally, at 85℃ for 5 minutes before the temperature was stabilized at 4℃.

Prior to the running of the PCR reaction, all samples were diluted in H_2O to a final concentration of 0.5 $ng/\mu l$ cDNA. The diluted cDNA was mixed with a Master Mix from TaqMan^{TM} Gene Expression Assay (Applied Biosystems^{TM}, ThermoFisher Scientific) containing a dye label (FAM) probe, a minor groove binder (MGB) probe, and a non-fluorescent quencher. Four genes were analyzed for quantitative measurement of their expression: OCT4 (POU5F1), SOX9, VCAN, COL2B, as well as the reference gene CREBBP. The two samples originated from the microtissues that had been cultured for 3 months were compared with 1 sample of chondrocytes that had been cultured as pellets and 1 sample of iPS cells from the established cell line A2B. The gene expression was studied with Real-Time PCR, for program specifications see Figure 3.9.

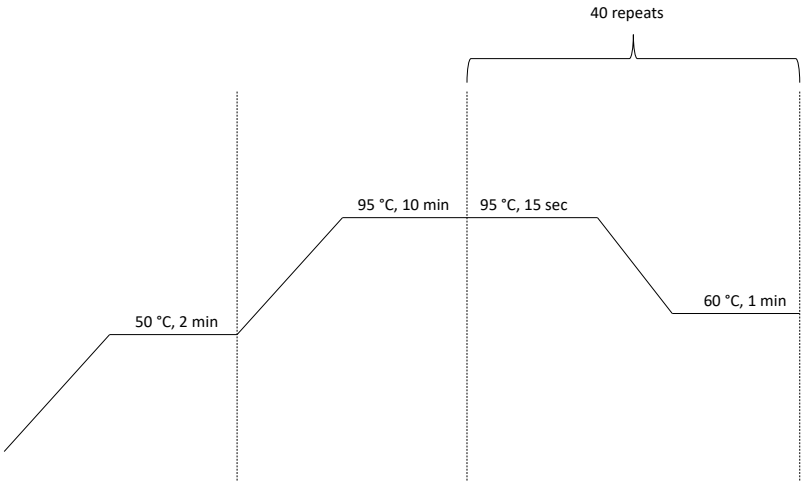

Figure 3.9: The running program for the Real-Time PCR.

3.7 Screening for ACAN Induction or Inhibition

Cells from the modified iPS cell line (H8) were subjected to screening in an In Cell Analyzer 6000 (GE Healthcare). Both screening of 1 field as well as 25 fields were subjected to the two different 96-well plates with H8 microtissues exposed to molecules. The screening with the In Cell Analyzer 6000 was performed with the objective Nikon® 10x, the optical resolution 500 nm, a Z step size of 2 μm, and the emission FITC, excitation blue. A library of FDA-approved molecules (Prestwick

Chemical) was screened together with the cells in order to search for possible aggrecan inducers or inhibitors. Prior to the screening, cells from the modified cell line H8 were cultured in a microwell culture plate for 3 days to allow for the transformation into microtissues. The procedure of seeding the cells in a microwell culture plate as well as the harvesting process after 3 days is described in Section 3.3.4. The formed microtissues were transferred to two 96-well plates with a cell density of approximately 23 microtissues per well (10,000 cells/microtissue). To allow for both the differentiation of iPS cells into chondrocytes and the initiation of aggrecan production, the 2 plates were incubated in a shaking incubator at $37°C$, 5% CO_2 and 30 rpm for 4 weeks with a pellet medium change 3 times per week.

Molecules (Prestwick Chemical) diluted in pellet medium to a concentration of 100 μM were added to the microtissues after 4 weeks of cell culturing and then continuously 3 times per week. Columns 1 and 12 on both plates were free from molecules and the microtissues in these wells were given nothing but medium (pellet medium). Hence, 2 columns on each plate could be analyzed as controls. The screening was carried out 1 week after the first addition of molecules and thereafter continually once every week for 4 weeks. The expectation from the screening process was to be able to distinguish whether the aggrecan production had been induced, inhibited or if it remained unchanged after the addition of the molecules. Since the H8 cell line is modified to express GFP under the ACAN promotor the discernment was based on the difference in fluorescence emitted from the cells.

4

Results

The resulting outcome of the different methodologies within this research project are presented here to provide an overview, thus contributing to evaluation and conclusion.

4.1 Optimization of Bioink

The optimization of the bioink process can be classified in three sections. Firstly the 60/40 NFC/A (% *w/w*) was compared to a lower and a higher NFC ratio as the alginate concentration was kept constant in a non-sterile environment, thus being evaluated together with 48/52 and 80/20 NFC/A (% *w/w*). Secondly, the bioinks were processed with an aseptic technique utilizing sodium alginate and NFC sterilized by autoclave. Lastly, the autoclaved sodium alginate was substituted with the purchased sterile PRONOVA SLG100 alginate due to observed weight loss and thinner bioink properties when autoclaved sodium alginate was applied.

4.1.1 Printability Test

Diameter variation measurements were performed to compare the shape fidelity and stability of the bioinks after bioprinting. The bioinks were printed as squares of 10×10 mm in one layer before the diameter and the corner length of the prints were measured with the Nikon® Eclipse Ti Series microscope and measurement tool. The diameter of the extrusion nozzle was 410 µm and the parameter settings such as pressure and speed were identical for all three bioinks. Despite the equally set parameters when printing with the different bioinks, the final constructs proved to differ in size. The result reveals a decrease in diameter and corner length with an increase in NFC quantity. Thereby it can be concluded that the shape fidelity and stability of the prints are enhanced with increasing amounts of NFC in the bioink.

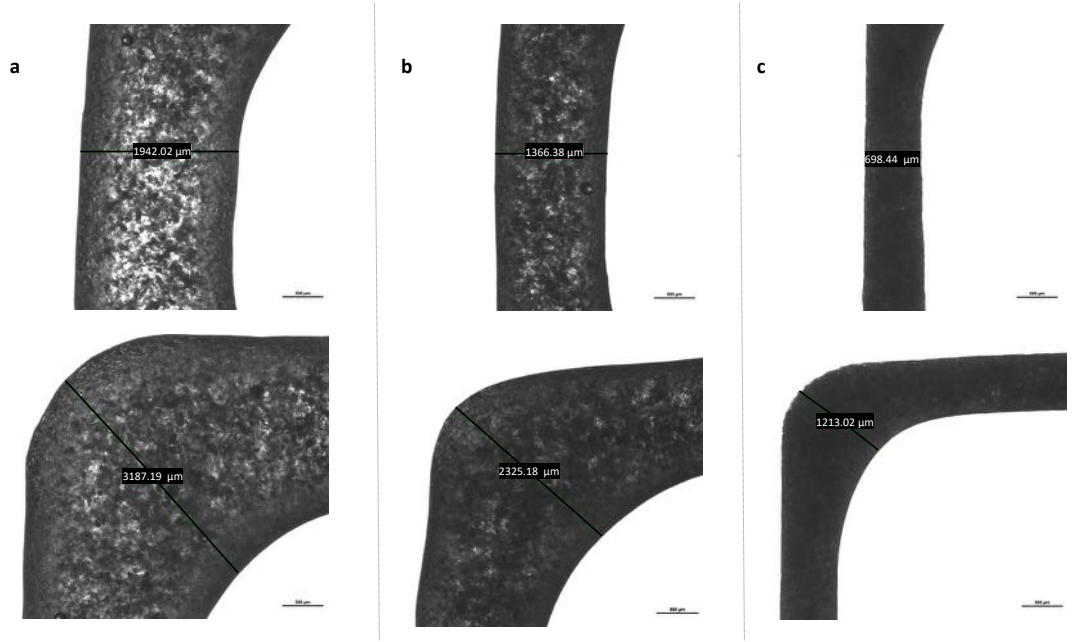

Figure 4.1: The diameter and the corner length of squares 3D printed with 3 different bioinks; 48/52 (a), 60/40 (b) and 80/20 (c) NFC/A (% w/w).

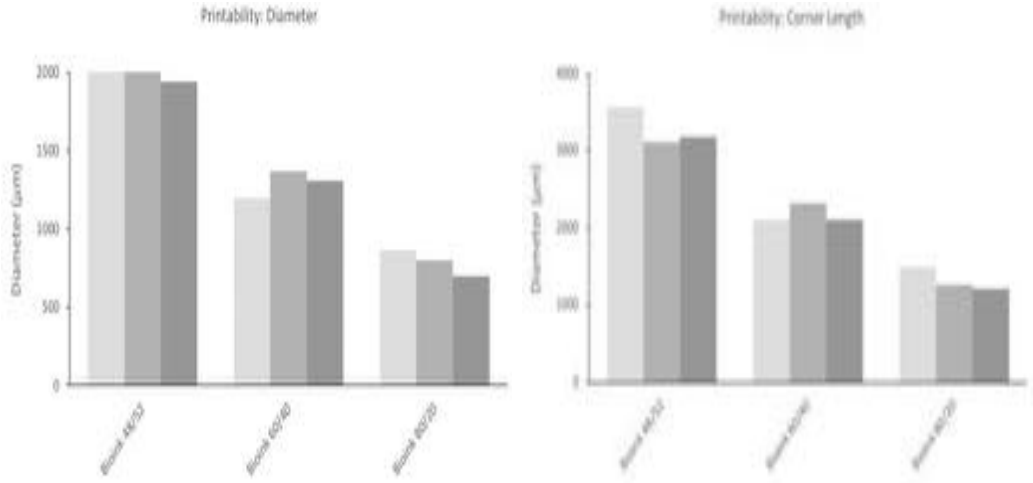

Figure 4.2: Diameter in the left diagram and corner length in the right diagram of 3D bioprinted squares with 3 different bioinks; 48/52, 60/40 and 80/20 NFC/A (% w/w), 3 replicates of each bioink.

The printability of the bioinks was supported with prints of a more complex shape than the previously mentioned squares. The three different bioink combinations were printed in S-shapes of three layers. Figure 4.3 visualizes the two S-prints of each bioink with 80/20 NFC/A (% w/w) to the left, 60/40 NFC/A (% w/w) in the middle, and 48/52 NFC/A (% w/w) to the right. The bioink 48/52 is unable to maintain a proper S-shape when printed in three layers. The two other bioinks

(60/40 and 80/20), however, are superior in shape fidelity and stability compared to 48/52 NFC/A (% w/w). A comparison of 60/40 and 80/20 NFC/A (% w/w) shows merely a slight disparity between the two bioinks where 80/20 NFC/A (% w/w) exhibits a somewhat higher shape fidelity.

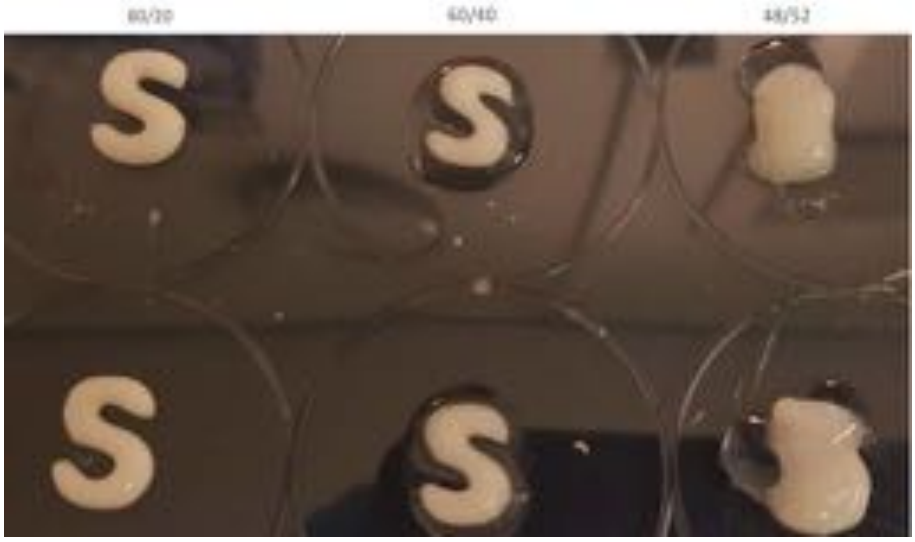

Figure 4.3: Printability test of the three bioinks; 80/20, 60/40 and 48/52 NFC/A (% w/w), printed in S-shapes in three layers.

4.1.2 Rheology

For further evaluation of the printability of bioinks the rheological properties were examined. A shear-thinning property is desired as low pressure used while 3D bioprinting increases the viability of the living cells. The graph of viscosity ($Pa \times s$) versus shear rate (s^{-1}) resulted in an overview of the rheological properties of the seven different bioinks analyzed, see Figure 4.4.

The bioinks 48/52 and 60/40 NFC/A NFC/A (% w/w) are following the same trend, both having a low viscosity relative to the other five bioinks being compared. The autoclaved 80/20 NFC/A (% w/w) bioink and the 60/40 NFC/A (% w/w) with the CELLINK LAMININK 521 as the NFC source and PRONOVA SLG100 alginate are similar in behavior. Pure alginate and autoclaved alginate bioinks differ regarding the rheological property viscosity, the autoclaved alginate bioink resulting in a lower viscosity. The 60/40 NFC/A (% w/w) bioink with autoclaved NFC and PRONOVA SLG100 alginate used for the small scale meniscus 3D bioprint results in a viscosity closest to the pure alginate bioink. The pure alginate bioink shows the highest initial viscosity that decreases to the same level as the 48/52 and 60/40 NFC/A (% w/w). All seven bioinks present a shear-thinning behavior, decreasing in viscosity while exposed to an increasing shear rate.

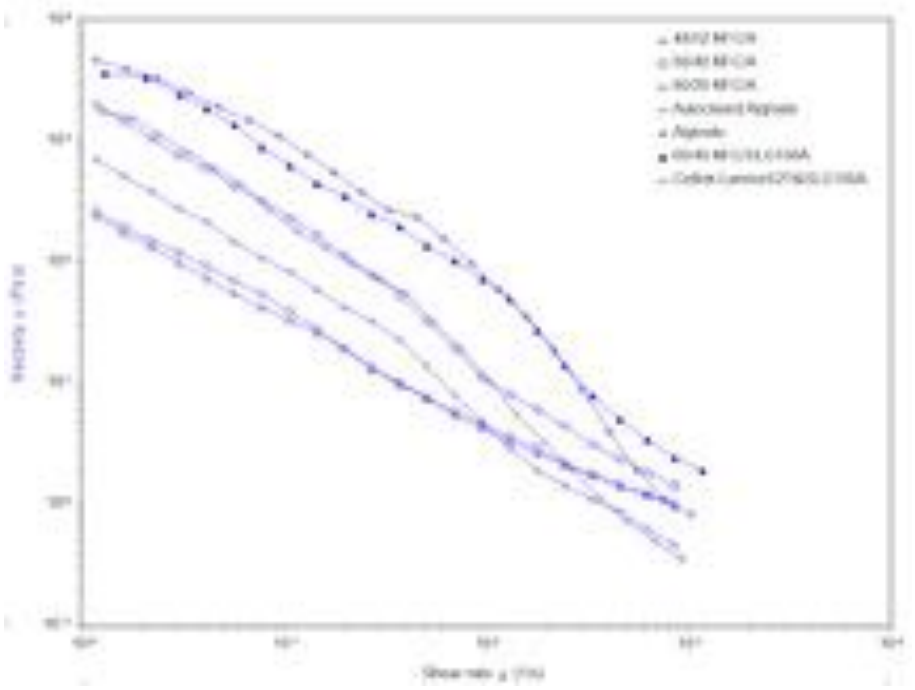

Figure 4.4: Rheological properties at 25°C for seven different bioinks: Autoclaved 48/52, 60/40 and 80/20 NFC/A (% w/w), Autoclaved alginate bioink, alginate bioink, 60/40 autoclaved NFC/ PRONOVA SLG100 alginate (% w/w) and 60/40 CELLINK LAMININK 521/ PRONOVA SLG100 alginate (% w/w).

As the 60/40 NFC/A (% w/w) had been compared to the 48/52 and the 80/20 NFC/A (% w/w) non-sterile bioinks the three ratios were produced with an aseptic technique. The bioinks produced with the sodium alginate and NFC sterilized by autoclave resulted in a thinner characteristic, thus a lower viscosity. The sodium alginate was observed to result in a weight loss after the autoclave process, hence considered to be the origin of the arising difficulties when printing. The sodium alginate was substituted with the purchased PRONOVA SLG100 alginate. The difference in printability and shape fidelity can be seen in Figure 4.5.

Both images visualizes a 3 mm small scale menisus. A 3D bioprint with sodium alginate to the left and PRONOVA SLG100 as an alginate source to the right. The meniscus structure has a firmer shape fidelity displayed in the image to the right.

Figure 4.5: A small scale 3 *mm* meniscus 3D bioprinted with 60/40 NFC/A (% *w/w*) sterilized by autoclave to the left. A small scale 3 *mm* meniscus with the PRONOVA SLG100 alginate, to the right.

4.2 Viability Tests

The results of the four cell viability in bioink evaluations are presented in the following section.

4.2.1 Cell Viability - Monolayer

The cell viability of iPS cells in the three different bionks was first evaluated simply by the addition of a layer of each bioink on cells seeded in monolayers in two 6-well plates. The initial quantity of cells added to each well was 100,000. Subsequently, the number of cells in each well was counted after one day of bioink exposure. Figure 4.6 displays an increase in cell count in the control samples seeded on plate 2. In the control wells, the number of cells was expected to increase since these wells only contained cell medium provided in order for the cells to grow until the well-surface was covered. The control sample on plate 1, however, does not meet the same expectations. Instead, the cell number has decreased. The same applies to the other wells on plate 1, they all present a lower amount of cells after bioink exposure. When comparing the samples on plate 2 it is evident that the bioink has some sort of negative effect on cell growth. A slightly higher cell count can be discerned in bioink 60/40 NFC/A (% *w/w*) compared to bioink 80/20 NFC/A (% *w/w*).

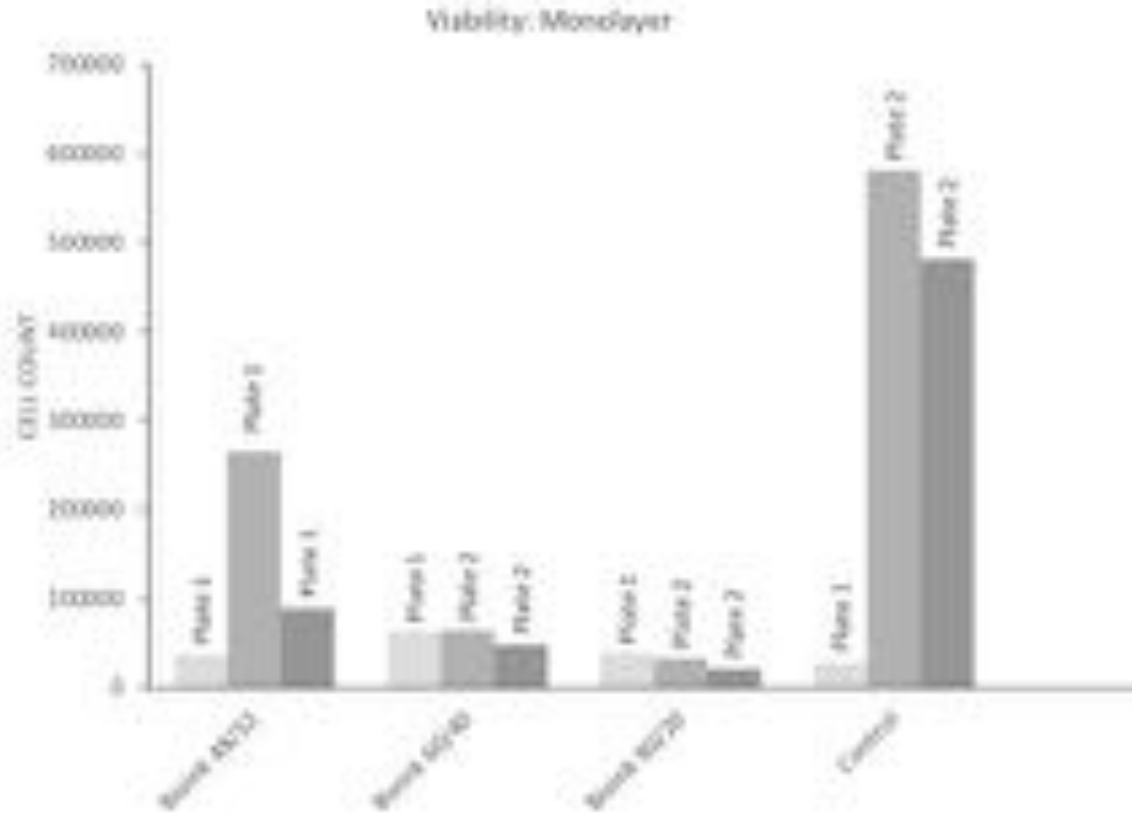

Figure 4.6: Viability measurements of cells after 1 day of bioink exposure. Three replicates of the control samples and each bioink; 48/52, 60/40 and 80/20 NFC/A (%w/w) divided on two 6-well plates.

4.2.2 Cell Viability - Pellets

Cells cultured as pellets in a 96-well plate were exposed to a layer of 200 µl of the three different bioinks; 48/52, 60/40 and 80/20 NFC/A (% w/w), three replicates for each bioink. Additionally, three samples containing nothing but a pellet and pellet medium were used as controls. After 8 days of bioink exposure, the pellets were separated from the bioinks and treated with Collagenase II in order to obtain a single-cell solution possible to count with a Bürker Chamber. The results from the cell count are displayed in Figure 4.7. The initial number of approximately 200,000 cells per pellet has diminished significantly in each sample, including the controls. The low cell number in the control samples is contradictory to the expectations since the number of cells in the controls were thought to remain unchanged at 200,000 cells per sample. The cell viability does not differ remarkably between the samples with the exception of bioink 48/52 NFC/A (% w/w) and one of the replicates of bioink 60/40 NFC/A (% w/w) that attain the foremost cell survival.

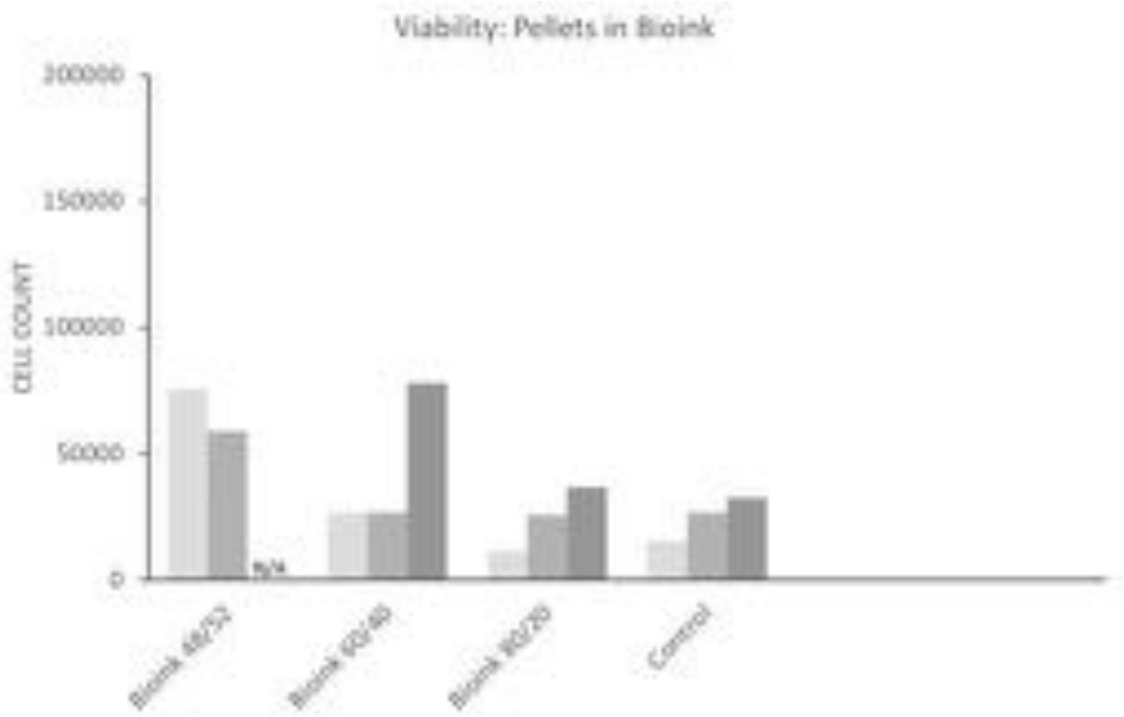

Figure 4.7: Cell pellets exposed to bioinks and counted after 8 days. Three replicates for each bioink; 48/52, 60/40 and 80/20 NFC/A (%w/w) and three controls. The cell number for each sample was counted with Bürker Chamber, one replicate of 48/52 NFC/A (% w/w) was not countable.

4.2.3 Cell Viability - Cells in Bioink

A cell viability test for single cells in a 3D environment, consisting of bioink, was obtained. The cell suspension/bioink ratio used was 3:10 resulting in each well in the used 48-well plate containing 289,000 single cells with a total cell suspension/bioink volume of 200 µl.

The three bioinks were divided into five wells respectively, concluding a total cell amount of approximately 1,4 $\times 10^6$ cells when the replicates are pooled. The single cells were counted with Bürker Chamber method, see Table 4.8. The cell viability was determined by the cell concentration obtained from the Bürker Chamber method. The outcome shows the bioink 60/40 NFC/A (% w/w) having slightly higher cell viability of 10,4% after 8 days in bioink. The survival of cells is visualized in Figure 4.8. The overview of cell viability can conclude a similar steep decrease for all three bioink ratios.

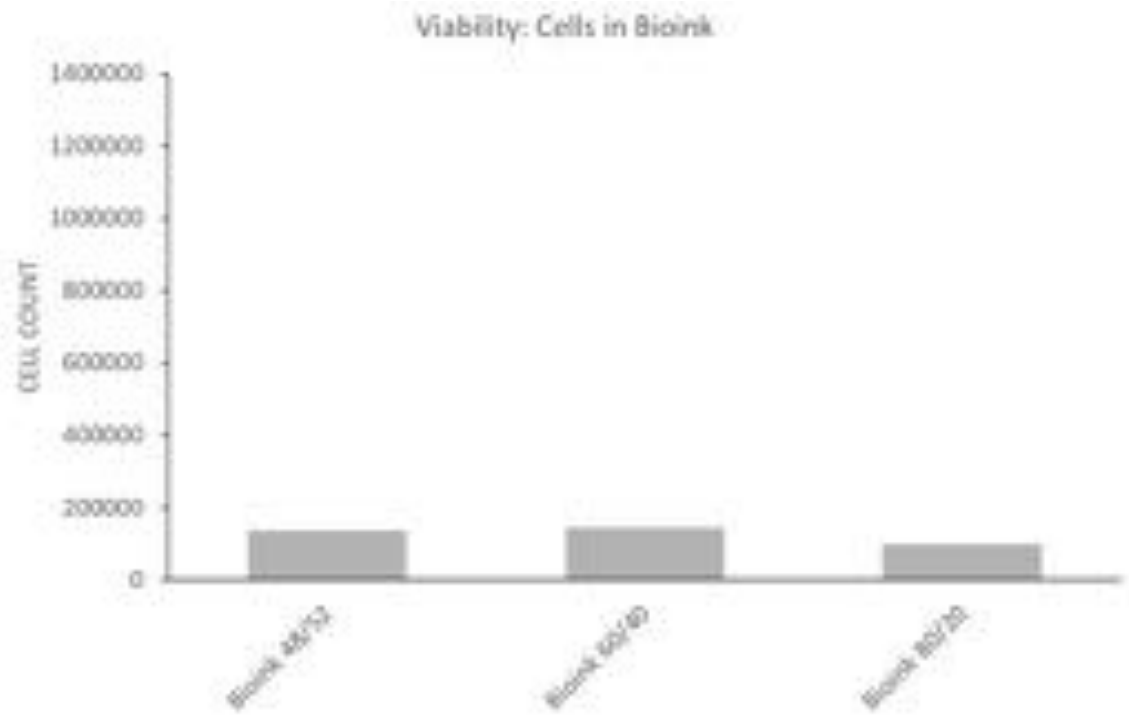

Figure 4.8: The cell viability after 8 days of bioink exposure.

4.2.4 Cell Viability - Bioprint

The cell viability of the microwell cultured cells utilized when 3D bioprinting constructs were analyzed. The mixture of the microtissue-suspension and bioink constructs were incubated and live-cell imaging with confocal microscopy of the samples was obtained at 1, 4, and 5 weeks after 3D bioprinting the 3 mm meniscus constructs, see Figure 4.9.

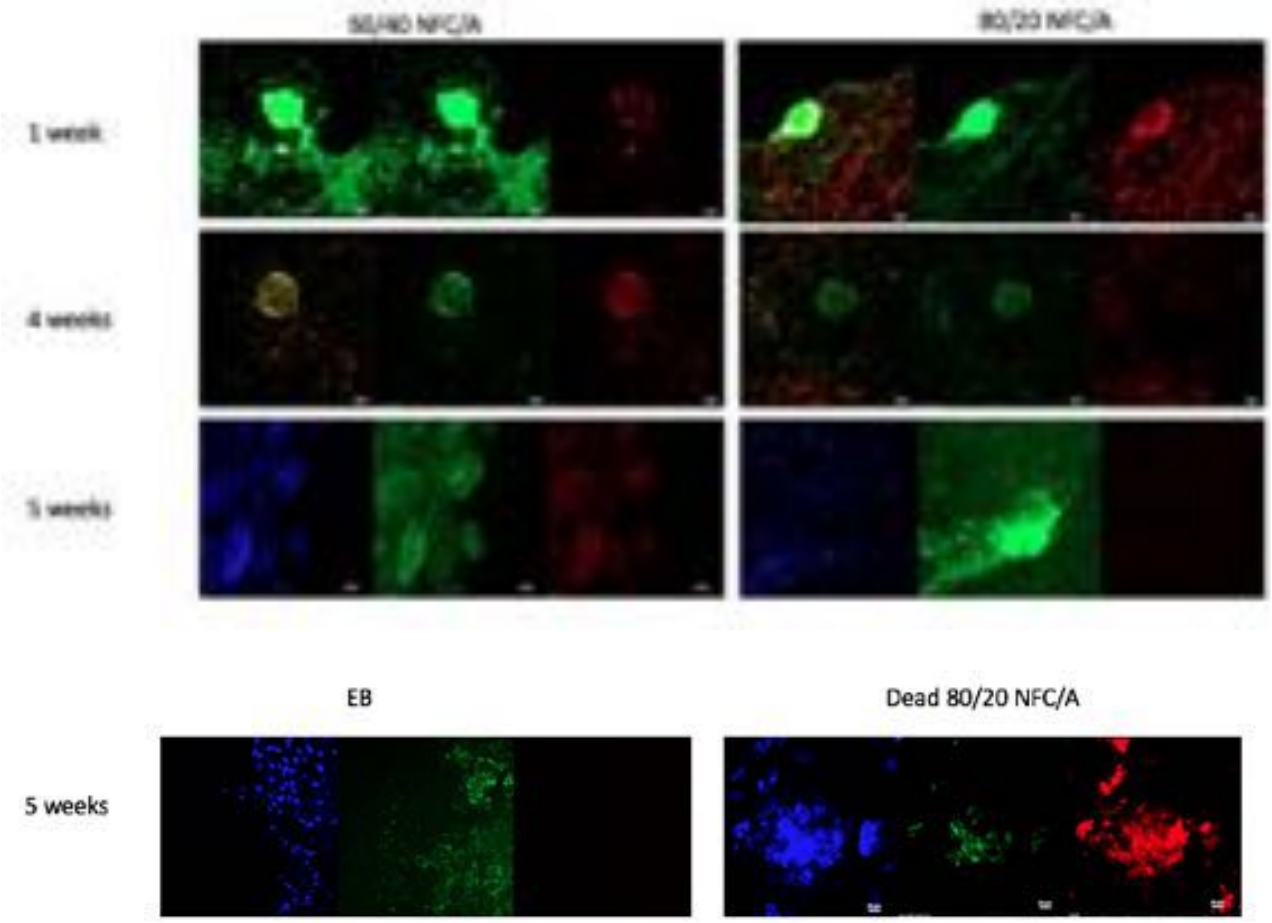

Figure 4.9: LIVE/DEAD® imaging by confocal microscopy of microtissues in bioprints of 60/40 and 80/20 NFC/A (% w/w) bioink, obtained after 1 week, 4 weeks, and 5 weeks. Further, confocal images of an microtissue and a dead sample were attained.

The viability assay with LIVE/DEAD® staining resulted in green and red fluorescence, where the green fluorescence represents the viability of cells and the red fluorescence present the dead cells. After the 3D bioprinted constructs had been incubated for one week the microtissue visualized in Figure 4.9 presents slightly higher viability in the bioink 60/40 NFC/A (% w/w) than in 80/20 NFC/A (% w/w) where the intensity of the red fluorescence is higher. A quantitative comparison between the two bioink ratios is difficult to obtain as the cell viability is hard to count with the resulting images. What can be concluded is that the microtissues are viable when mixed with bioink, 3D bioprinted, and incubated in 37°C and 5% CO_2. After five weeks the constructs received an additionally stain, DAPI, were used to visualize the cell nucleus in both live and dead cells. The confocal image of just an microtissue visualizes viable cells. The dead control of an microtissue immersed in bioink 80/20 NFC/A (% w/w) exposed to 75% ethanol in -20°C shows an intense red fluorescence, thus an equitable representation of non-viable cells. The

fluorescent milieu surrounding the intense luminescent microtissues is considered to be NFC.

4.3 3D Bioprinting Meniscus

A microtissue immersed in bioink, bioink number 6 in Table 3.4, and 3D bioprinted is visualized in Figure 4.10. The image shows a microtissue in the 60/40 NFC/A (*% w/w*) that is still intact. The microtissue consists of cells (dark dots) surrounded by connective tissue (stained blue). The result indicates a possibility of 3D bioprinting microtissues obtained with 3D culturing of iPS cells in microwell culture plates.

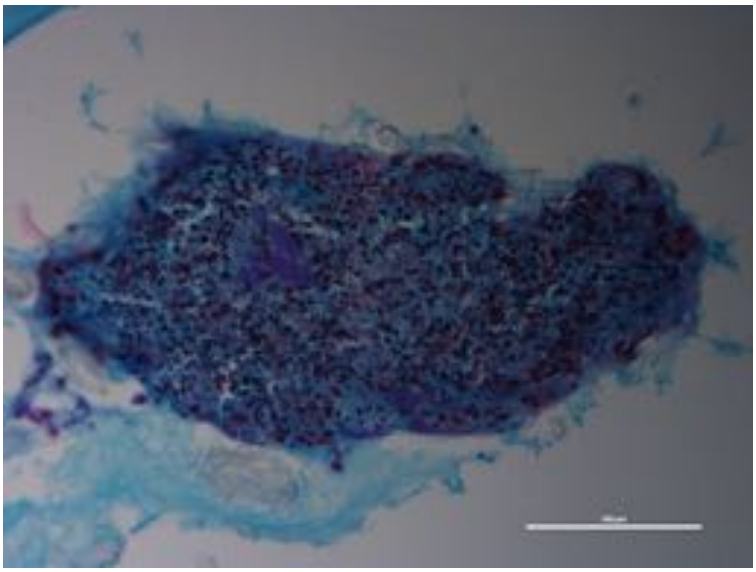

Figure 4.10: Alcian blue van Gieson stained paraffin-embedded microtissue 3D bioprinted with 60/40 NFC/A (*% w/w*).

4.3.1 Live/Dead Staining

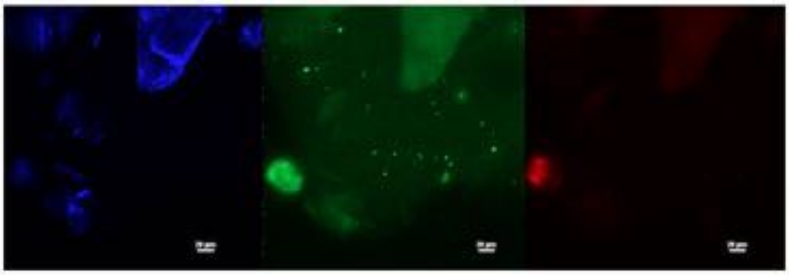

Figure 4.11: 3D bioprinted small scale meniscus. Stained and studied in confocal microscope 1 week after bioprinting (bioink number 6 in Table 3.4).

To the left one can presume a small part of a microtissue as the DAPI visualizes staining of nuclei. The middle image reveals an intense green fluorescence and the image to the far right shows a small part of the presumed microtissue to be nonviable.

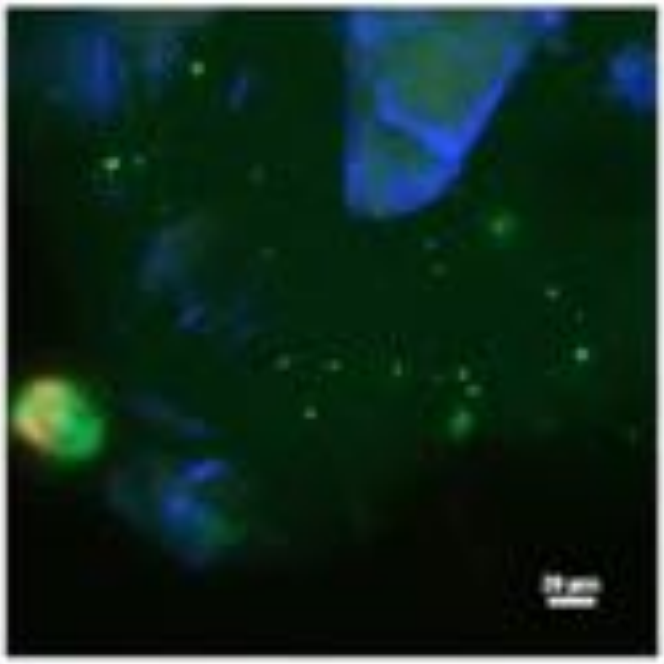

Figure 4.12: 3D bioprinted small scale meniscus. Stained and studied in confocal microscope 1 week after bioprinting (bioink number 6 in Table 3.4).

When analyzing the small part of the assumed microtissue one can observe a larger amount of viable cells in the bioink 60/40 NFC/A (*% w/w*), the NFC source being autoclaved and the alginate used is the PRONOVA SLG100.

4.4 3D Bioprinting for Transplantation

The first trial of 3D bioprinted constructs for implantation in mice was performed with bioink printed as droplets on COPLA Scaffolds^{TM} and microtissues were immersed in between. The implants were transplanted in 18 mice with two implants in each. The implants were *in vivo* cultured in mice for five weeks. The explanted implants appeared to have had cartilaginous tissue generation as the constructs resemble cartilage structure in comparison to the more fragile texture before implantation.

Figure 4.13 shows one of the 3D bioprinted constructs, loaded with an anti-metastatic drug and Nile RED, from the second trial. This implant has not been transplanted into mice. The image displays the paraffin-embedded section for analysis.

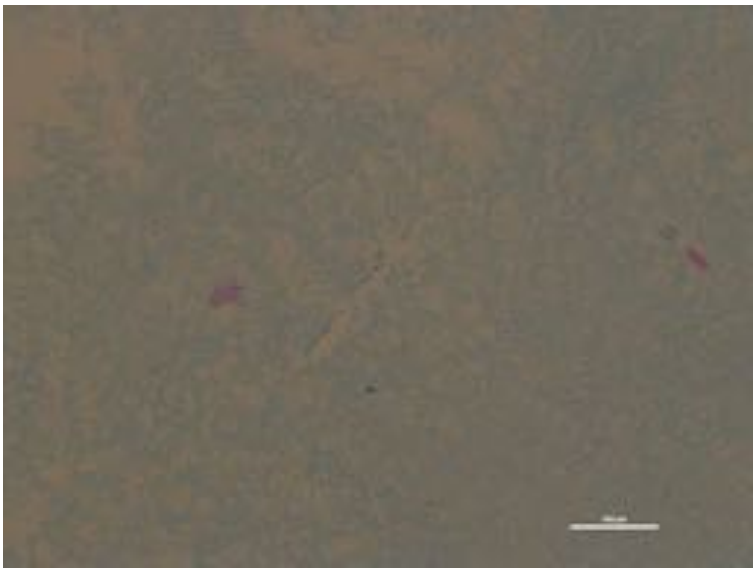

Figure 4.13: A 3D bioprinted construct with 60/40 NFC/A (*% w/w*) with microtissues cultured from the cell line H8 and loaded with anti-metastatic drug and Nile RED.

4.5 Differentiation of iPS Cells in 3D Cell Culturing

Surplus microtissues from the established cell line A2B were cultured and evaluated for 3 months. Morphological analysis, immunohistological assay, and real-time quantitative reverse transcription-PCR were performed to gain a deeper understanding of the differentiation of iPS cells cultured as microtissues.

4.5.1 Morphology

The evaluation of cell morphology resulted in a visualization of the different cells showing diversity in appearance. The A2B cell line cultured for three days can be seen to the left in Figure 4.14. The image shows cells with round shapes, large nuclei, and merged cytoplasm, features that are typical for iPS cells. Microtissues cultured for 2 months and enzymatically treated to form a single-cell suspension are displayed to the right in Figure 4.14. The structure of these cells indicates that the cells have undergone differentiation towards chondrocytes. The morphology is more elongated compared to the iPS cells.

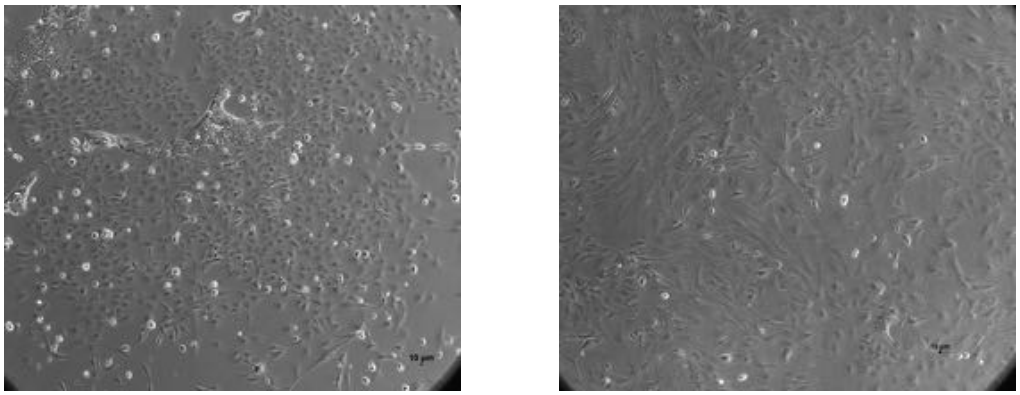

Figure 4.14: To the left, iPS cells cultured in a cell culture flask for three days. To the right, microtissues treated with a collagenase digestion cocktail and seeded for six days in a cell culture flask.

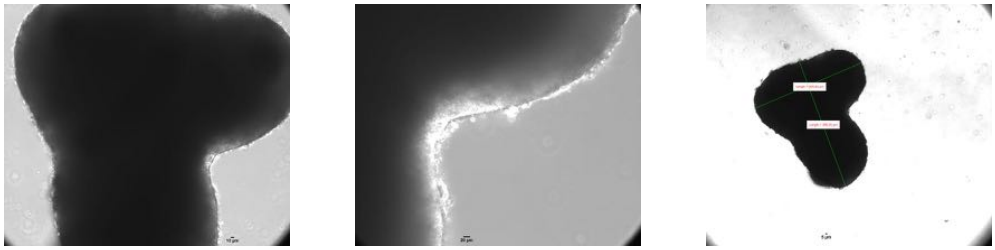

Figure 4.15: An A2B microtissue measured to a length of 396.05 µm and a width of 345.60 µm, after 2 weeks of incubation.

The A2B cell line showed great potential in forming microtissues and generating ECM. The image below visualizes the A2B microtissues cultured for two months. These are the microtissues utilized in both 3D bioprinting meniscus and the first trial for transplantation, see Figure 4.16.

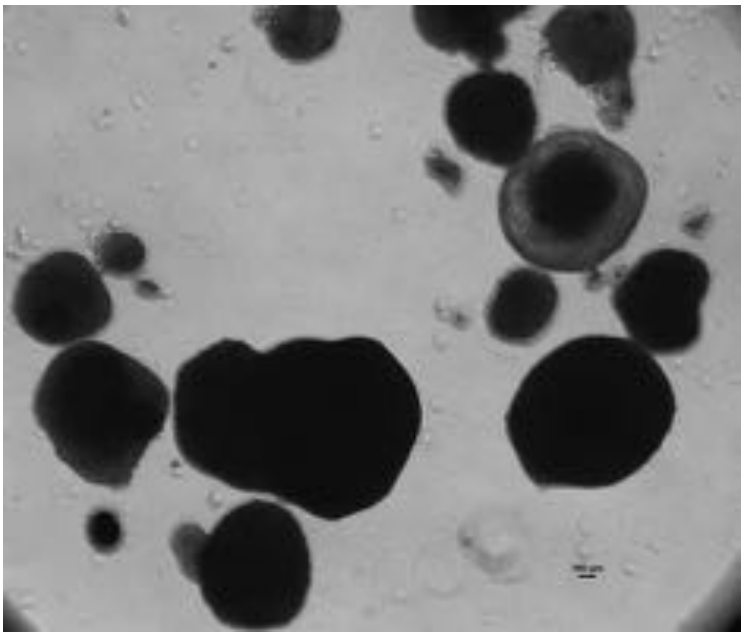

Figure 4.16: A2B microtissues cultured for two months displaying the ECM formation with a scale bar of 100 µm displayed in the lower right corner.

4.5.2 Immunohistology

The two-month cultured microtissues were evaluated by visualizing the structure with the Alcian blue van Gieson stained paraffin-embedded sections. Within the ECM, the collagen is stained red/pink and the proteoglycans appear blue. The cell nuclei are seen as darker dots, see Figure 4.17.

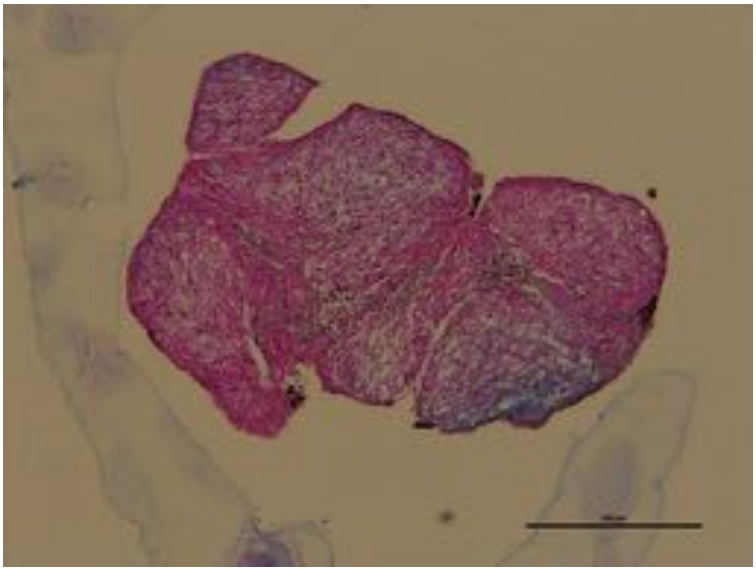

Figure 4.17: Alcian blue van Gieson stained paraffin-embedded microtissue section. Cells (dark dots) dispersed in a network of connective tissue (pink).

The microtissue section was obtained to evaluate the ECM formation and generated

a feasible further evaluation of antibody staining to advance the evaluation of the composition as the cartilage matrix is composed of glycosaminoglycans, proteoglycans, elastin and, collagen fibers. An enlargement of the microtissue section can be seen in Figure 4.18.

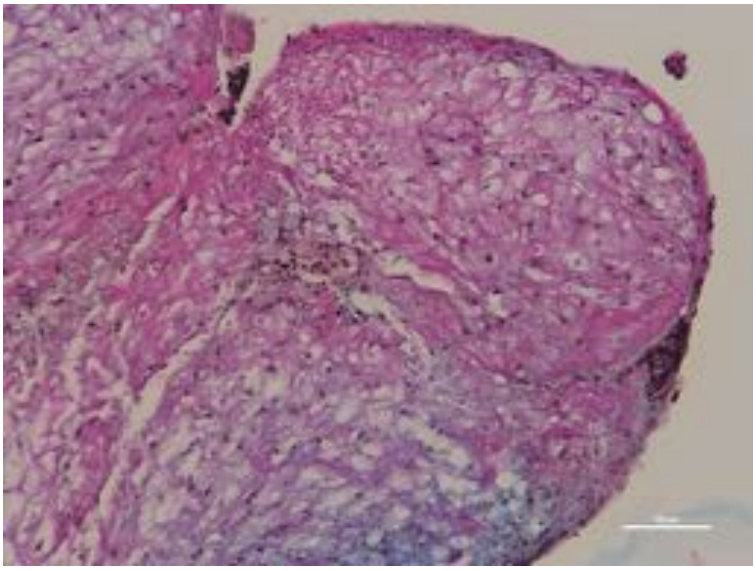

Figure 4.18: An enlargement of the Alcian blue van Gieson stained paraffin-embedded microtissue section with cells visualized as dark dots and connective tissue is colored pink.

Chondrocytes produce varying amounts of collagen depending on the cartilage type. Further analysis of the collagenous extracellular matrix is of interest to evaluate the composition of microtissues. Immunohistochemical staining for collagen type II was performed on the microtissue section as well as a positive and a negative control, both consisting of chondrocytes. The negative control disappeared during the staining procedure and was not able to be visualized. In the positive control sample (Figure 4.19), the cells (blue stain) are situated close to one another. The collagen type II (red stain) is intense on the outer parts of the section.

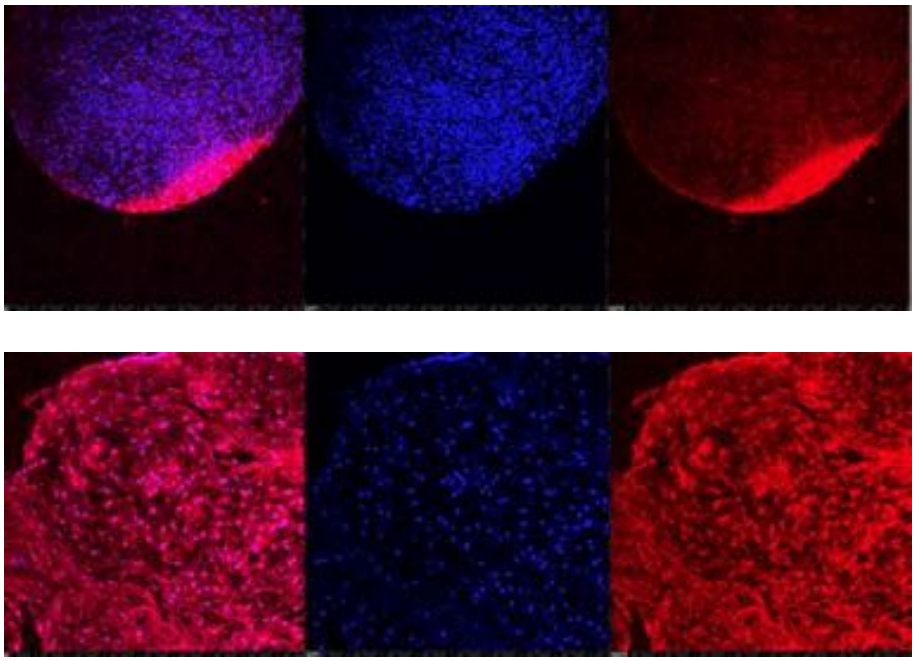

Figure 4.19: Confocal microscopy image of a section of chondrocytes (blue) used as positive control. The section is stained for collagen type II (red) and visualized at 10X and 20X respectively.

Figure 4.20 displays a section of a microtissue, stained for collagen type II. Compared to the positive control, the cells in the microtissue are more separated, enabling the formation of a well-distributed network of collagen type II. The immunohistochemical analysis further proves the differentiation of iPS cells cultured as microtissues.

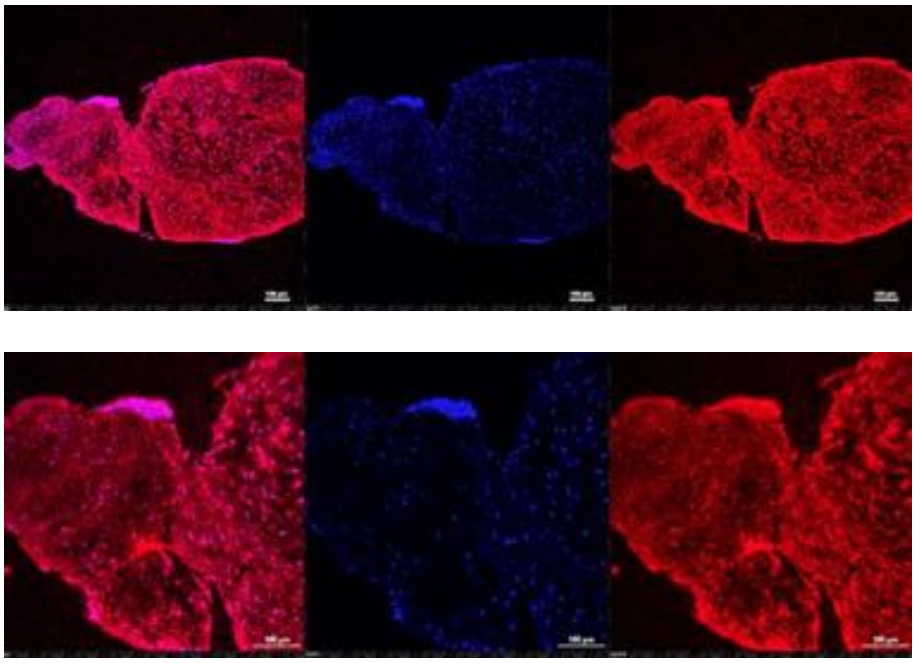

Figure 4.20: A section of a microtissue exposed to immunohistochemical analysis. Cell nuclei in blue and collagen type II in red. The images are captured with confocal microscopy at 10X and 20X.

4.5.3 Real-Time Quantitative Reverse Transcription-PCR

Four genes of interest were analyzed with Real-Time PCR, all genes were normalized to CREBBP. The sample with iPS cells was used as a control for the gene expression of stem cells while the chondrocyte pellet represented chondrocyte controls. OCT4, encoded by the POU5F1 gene, is a transcription factor involved in the maintenance of the pluripotency of stem cells. As expected, the expression of OCT4 is extensively higher in the iPS cells compared to the chondrocyte pellets, to the left in Figure 4.21a, where the expression is almost zero. The same accounts for the expression of OCT4 in the microtissues. The low values indicate that the cells in the microtissues have lost their pluripotency and differentiated toward chondrocytes. SOX9 is a transcription factor involved in chondrocyte differentiation and early cartilage formation. To the right in Figure 4.21a displays that the chondrocyte pellets possess the highest SOX9 expression closely followed by the two microtissue-samples. The expression of the gene VCAN, encoding the proteoglycan Versican that is present in the ECM, is superior in the chondrocyte pellets. The two microtissue-samples and the iPS cells exhibit similar expression levels of VCAN, to the left in Figure 4.21b. Collagen type IIB is a splicing variant of collagen type II and therefore usually found in mature cartilage. The most abundant expression of COL2B is the second microtissue-sample as well as in the chondrocyte pellets, to the right in Figure 4.21b. However, the great variation between the two microtissue-samples complicates the evaluation.

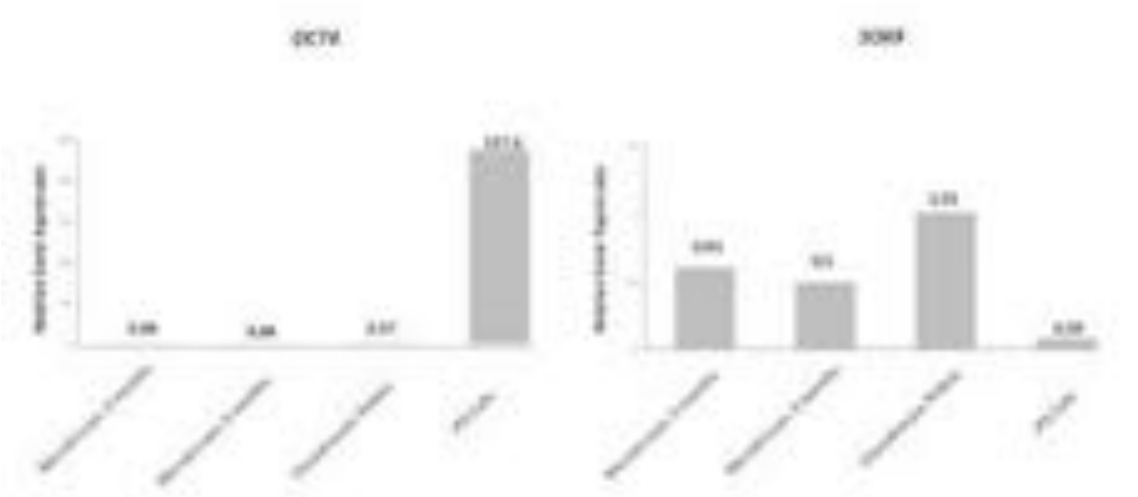

(a) Relative gene expression of *OCT4* and *SOX9*.

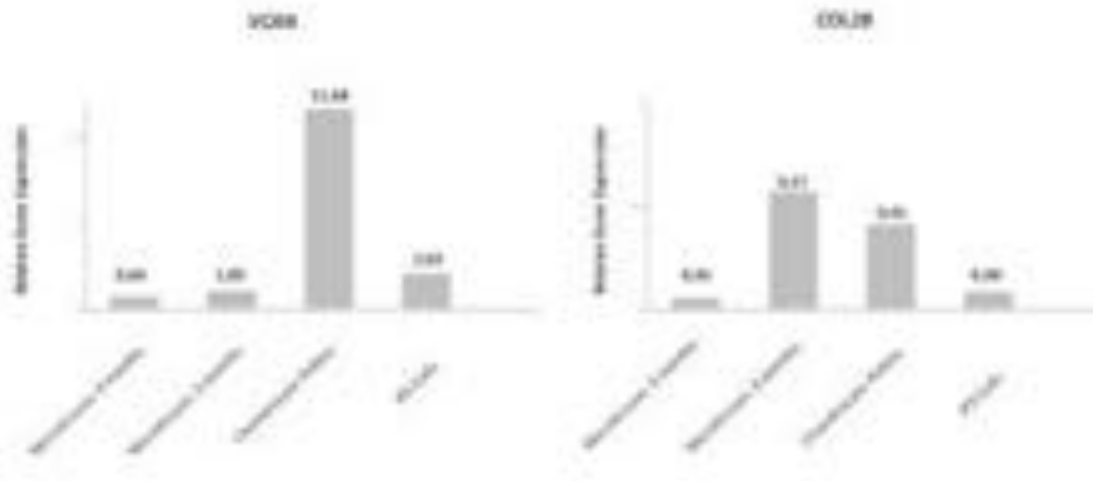

(b) Relative gene expression of *VCAN* and *COL2B*

Figure 4.21: Relative gene expression of OCT4, SOX9, VCAN and COL2B measured in two microtissue-samples, one chondrocyte pellets-sample and one sample with iPS cells. All genes have been normalized to the reference gene CREBBP.

4.6 Screening for ACAN Induction or Inhibition

Two 96-well plates containing microtissues of the modified cell line H8 were subjected to screening of a library of FDA-approved molecules. The initial screening was performed after 5 weeks of culturing as microtissues and 1 week after addition

of molecules. The screening process was carried out for a total of 4 times (week 5-8) per plate (plate 1-2).

Each well in plate 1 and plate 2 have been analyzed and compared over 4 weeks to distinguish any alteration in intensity. Figure 4.22 displays results from the screening of plate 1. Row F, column 2 exhibits an intense fluorescence while row C, column 3 is completely shut down. These wells have received molecules added as controls to verify the reliability of the screening.

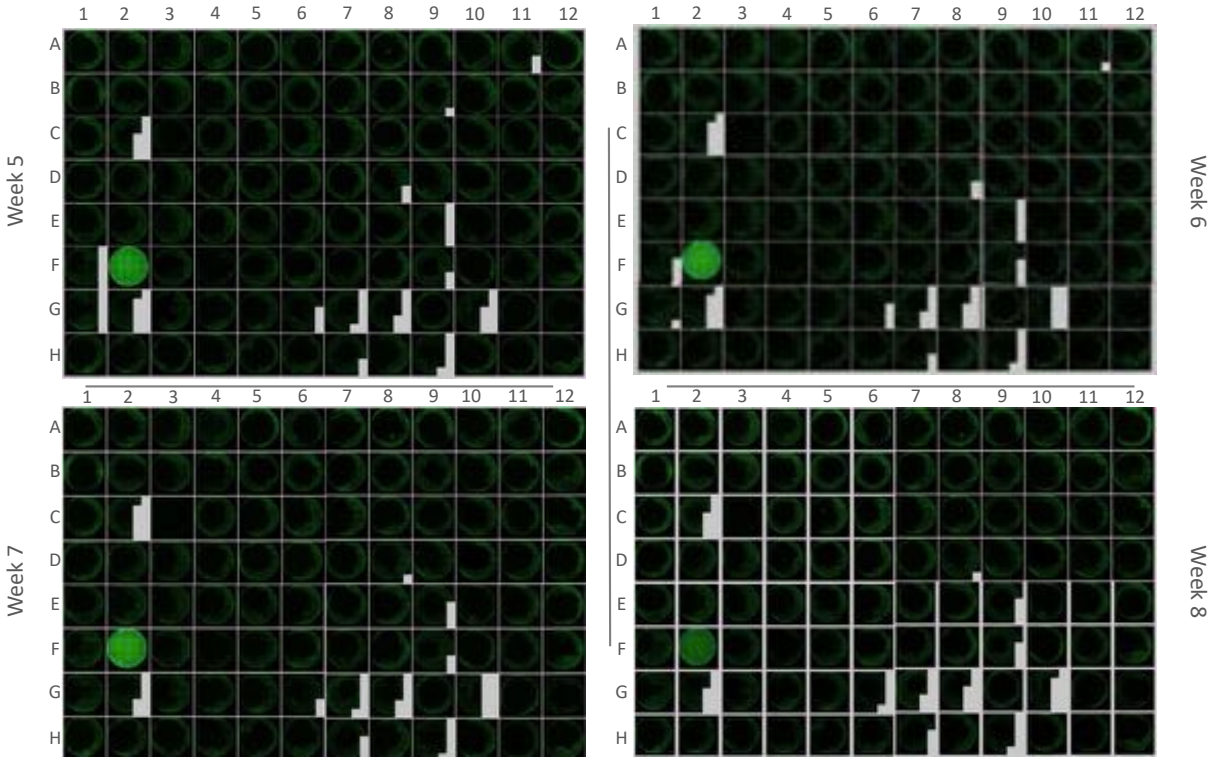

Figure 4.22: Plate 1: Cells modified to express green fluorescence protein under the ACAN promotor and cultured as microtissues in a 96-well plate. Molecules have been added to the wells to distinguish differences in intensity due to aggrecan induction or inhibition. The plate has been subjected to screening after 5, 6, 7 and 8 weeks of culturing as microtissues.

Plate 1 resulted in 5 wells indicating an induction as well as 4 wells expressing an inhibition of aggrecan production over the four weeks of screening. As the judgement was based on the difference in fluorescence emitted from the cells the results were obtained when comparing the intensity of green brightness.

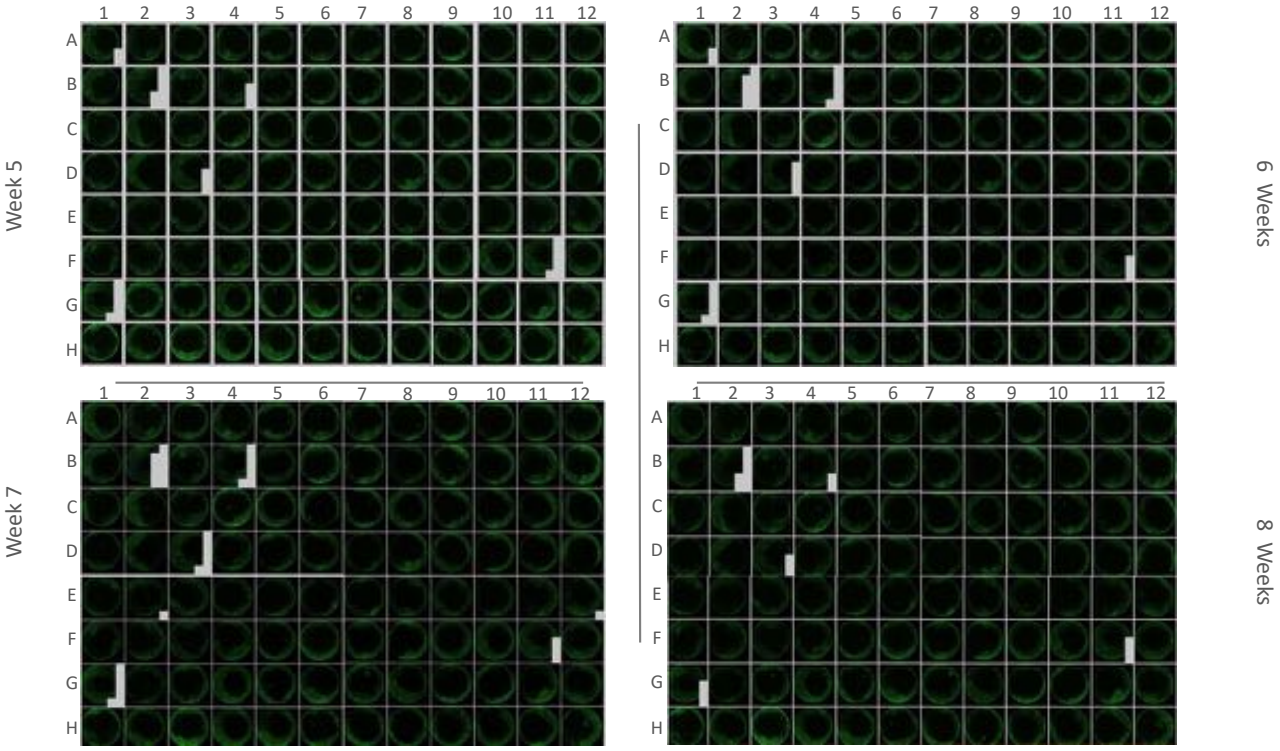

Figure 4.23: Plate 2: Cells modified to express green fluorescence protein under the ACAN promotor and cultured as microtissues in a 96-well plate. Molecules have been added to the wells to distinguish differences in intensity due to aggrecan induction or inhibition. The plate has been subjected to screening after 5, 6, 7 and 8 weeks of culturing as microtissues.

Plate 2 resulted in 3 wells indicating an induction as well as 2 wells expressing an inhibition of aggrecan production over the four weeks of screening.

The H8 cell line used throughout the screening did not result in the same uniform and intact microtissues as the A2B cell line, during the 3D culturing. The green fluorescence can therefore be a result of auto-fluorescence of non-viable cells separated from the microtissue, thus a disturbing background taken into account when comparing the well intensity.

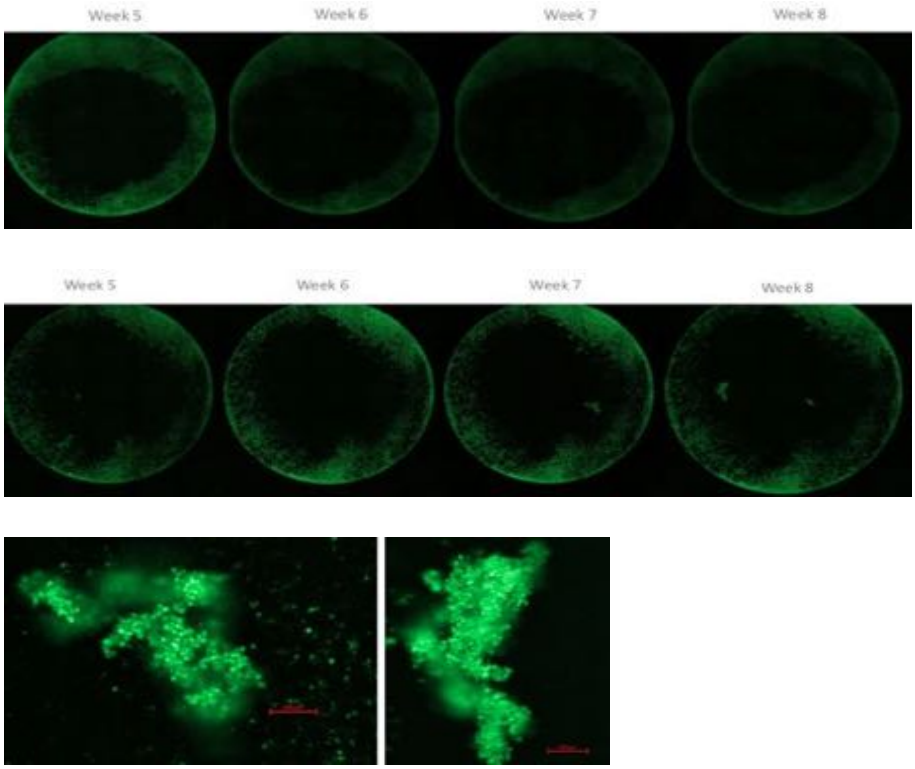

Figure 4.24: The screening resulted in decreased intensity in some wells and increased intensity in others. The figure displays screening result of plate 2 where the top 4 wells (G2) are indicating an inhibition of ACAN production from week 5 to week 8. The middle 4 wells (B9) instead exhibit an induction of ACAN production. The two bottom figures are a zoom in of the microtissues visualized in well B9, week 7 and week 8.

The two wells compared, Figure 4.24, gives a closer look of week 7 and 8 and visualizes formation of microtissue aggregates, which indicates induction of the aggrecan production. The upper picture displays the result of an inhibition and the middle image shows an induction of the aggrecan production over the four weeks of screening.

5

Discussion and Conclusion

One of the expected outcomes was an optimized bioink ratio with high printability, shape fidelity, and cell viability. A successful protocol production of the optimized bioink was also of interest. Another expectation was to differentiate iPS cells to chondrocytes by 3D culture and utilize these microtissues immersed in bioink while 3D bioprinting cartilaginous tissue. A screening of an FDA-approved library of small molecules to observe induction or inhibition of aggrecan production in microtissues, cultured with the iPS cells modified to express GFP under the aggrecan promotor, was evaluated with the ambition to obtain candidate molecules for at future OA cure. If the results have met the hypotheses are further discussed and followed by a conclusion.

5.1 Optimization of Bioink

The optimization of the bioink process can be classified in three sections. The ambition was to keep the alginate concentration constant at the percentage of 5,9%. This specific ratio has previously presented a high cell viability and previous research also provides results of a 60/40 NFC/A (% *w/w*) bioink being adequate to maintain a pluripotent phenotype after 3D bioprinting when using iPSC-conditioned medium (Nguyen et al., 2017). The expectation of the bioink 60/40 NFC/A (% *w/w*) being a good candidate to further evaluate was therefore established. A bioink requires the features of possessing a high viscosity for stability and shape fidelity with the balancing trait of retaining an environment for high cell viability. The first step in the estimation of producing the bioink was to conduct the bioink with a non-sterile technique to comprehend the characteristics of the ratios evaluated. The protocol of optimizing the bioink was originally established with a non-sterile method to interpret the chosen NFC/A ratios and to advance the protocol. When the procedure had been conducted repetitively and the shape fidelity, stability, and printability had been measured the optimization was directed towards the cell viability and the bioink was produced with aseptic technique.

The NFC and alginate were autoclaved to perform the sterilization of the components thus being the second step in the optimization of the bioink. New features of the bioink were obtained. An autoclave sterilizes by temperature and pressure and the alginate showed a weight decrease after being exposed to the aseptic procedure. The weight loss of the alginate was determined to 4-8% after repeating the

process, thus a weight addition was regulated before sterilization by autoclave. A hypothesis that the bioinks produced with this approach were to provide the same shape fidelity, stability and printability as the non-sterile bioink, remained despite the weight decrease. The three different autoclaved bioink ratios all resulted in a thinner condition, thus a decrease in the sought qualities. This resulted in the theory that the features of alginate were altered with the sterilization by autoclave, due to the observed weight decrease of alginate and the perception of a more diluted bioink result. Here the ratio of 48/52 NFC/A (*% w/w*) was discarded as this ratio obtained the least shape fidelity.

In a third method, with the objective to optimize bioink, the autoclaved alginate was replaced with highly purified PRONOVA SLG100 alginate. When neglecting the sterilization by autoclave step the 60/40 and 80/20 NFC/A (*% w/w*) ratios were to be compared. As previous research has shown the 60/40 NFC/A (*% w/w*) to hold higher cell viability than the 80/20 NFC/A (*% w/w*), this was the ratio chosen for further investigation. The rheological properties resulted in the autoclaved 80/20 NFC/A (*% w/w*) having a higher viscosity than the autoclaved 60/40 NFC/A (*% w/w*) as well as it resulted in a slightly favorable printability characteristic. The higher concentration NFC contributes to shape fidelity, stability, and printability. The autoclaved pure alginate also resulted in a low viscosity, actually the sample with the third lowest viscosity. The autoclaving is not a degradation tool itself but can engage in stimulating other degradation mechanisms thus resulting in a decreased swelling capacity and a reduced molecular weight (Cardoso et al., 2014). Despite this, the 60/40 NFC/A autoclaved NFC/PRONOVA SLG100 alginate resulted in a similar viscosity as the pure alginate and the bioink with the highest viscosity when comparing all seven samples, see Figure 4.4. The expectation of the bioink 60/40 NFC/A (*% w/w*) being a good candidate was met and chosen as the optimized ratio to proceed with. The optimization of bioink resulted in a solid protocol and a bioink candidate.

5.2 Cell Viability in Bioink

The cell viability in the various bioink ratios was measured by four approaches. Common for the four measurements was that they all eventuated in quantitative analysis with the objective to calculate live cells. In the initial viability test, cells were seeded in two 6-well plates and covered with bioink. In the control sample on plate 1, the cell number appeared to decrease. The cells in the control wells were supplied with medium and allowed to grow until they covered the entire well surface. Therefore the expectation was to witness an increased or unchanged amount of cells in the control samples. The unexpected result of the control on plate 1 contributed to difficulties in the analysis of the entire plate. It is challenging to interpret whether the decrease in cell count is due to the bioink exposure or if the low cell count in the control sample can be reflected in the adjacent wells. On the contrary, the control samples on plate 2 expanded until the entire well surfaces were covered. Accordingly, plate 2 is perceived as more reliable than plate 1. Although very small, a slightly higher cell number in bioink 60/40 compared to 80/20 NFC/A

(% w/w) can be distinguished. A continuous trend of a decreased amount of live cells in all three bioinks on both plate 1 and plate 2 is displayed. The result could be due to low acceptance of the cells towards the bioink constituents but it could also be a consequence of an obstructed accessibility of nutrients and oxygen through the compact bioinks covering the cells.

The second attempt at measuring the cell viability was conducted with pellets immersed in bioink. At first, it was thought that the pellets were to be found and simply separated from the bioinks. Unfortunately, the pellets could not be distinguished from the bioinks. Instead, the bioinks were dissolved with the addition of DPBS(-/-) and removed. The cells were separated with a collagenase II treatment and counted manually with Bürker chamber. Yet, residues of NFC remained in the samples and disturbed the cell counting process as it is difficult to discern cells from NFC. Moreover, the pellets require a more thorough treatment to completely separate the cells into a single-cell suspension. In the control samples, aggregates of cells remained even after treatment with collagenase II which hampered the counting process. This is a possible reason for the low cell count in the controls, samples that were expected to yield the highest numbers.

For the viability measurement of single-cell suspension mixed with the three bioinks, the initial plan was to use the cell counter to count viable cells. However, the bioinks did not dissolve properly. Remaining NFC was mistaken for cells and included in the cell counter. The resulting cell viability number was therefore not reliable. Instead, Bürkers chamber was employed for manual cell counting. The resulting cell viability, displayed in Figure 3.5 did not support the hypothesis as a cell count closer to the initial cell number was expected. The harsh process of dissolving the bioinks with DPBS(-/-) could have contributed to the resulting cell viability. Further, even when counted manually with Bürker chamber, the NFC disturbs and could conceal the live cells.

A final cell viability analysis was performed with microtissues 3D bioprinted as droplets. The comparison included only two bioink ratios; 60/40 and 80/20 NFC/A (% w/w) as 48/52 NFC/A (% w/w) had displayed poor shape stability when 3D printed. The 3D bioprinted droplets were stained and studied with confocal microscopy. The method did not give a quantitative result but it provided a general overview of the microtissues in the bioprints. The bioink 60/40 NFC/A (% w/w) were thought to provide a more favorable environment for the cells compared to the bioink 80/20 NFC/A (% w/w). One week and four weeks after bioprinting a slightly more intense green fluorescence could be distinguished from the microtissues in the 60/40 NFC/A (% w/w) bioink. Although, a more thorough and quantitative measurement is necessary to draw any conclusion of the cell viability.

To summarize the cell viability measurements, there is a need to develop a method to separate and distinguish cells immersed in NFC-based bioinks before counting the cells. The most reliable findings emerged from the bioprinted droplets studied with confocal microscopy. Although not quantitative, this method provides an insight

into the positioning and survival of microtissues.

5.3 3D Bioprinting Meniscus

Five menisci where 3D bioprinted with microtissues in 60/40 NFC/A (% w/w) bioink. One of the 3D bioprinted structures was subjected to staining and studied in a confocal microscope one week after bioprinting. The microtissues were not emphasized in the microscope and the cells were concealed by NFC in the bioprint. Figure 4.11 and Figure 4.12 reveal structures that remind of cells and microtissues. A more reliable method where cells are distinguished from NFC is required. Two of the menisci were sectioned and stained four weeks after bioprinting. The sections were studied microscopically and a microtissue could be displayed. In the microtissue, cells are dispersed in a network of connective tissue. Although a desirable result to be able to visualize cells and their ECM, the expectation was to see a more extensive amount of microtissues situated closer to one another. One possible approach to enhance the prevalence of microtissues in the bioprints would be to include more microtissues per ml bioink before bioprinting.

5.4 Differentiation of iPS cells in 3D Cell Culturing

The resulting microtissues of the A2B cell line were generating ECM with a distinct and marked encircling line correlating to a notable connective tissue production, see Figure 4.15. These small tissues visualize the iPS cells 3D cultured and differentiated into cells capable of producing ECM. It can be concluded that the iPS cells have the ability to differentiate when 3D cultured. The H8 cell line possessed poor capacity of forming microtissues. The H8 microtissues tended to dissolve and did not result in the same robust cultured tissues as the A2B cell line. The A2B microtissues were collagenase II treated to obtain single cells from the cultured tissue. This was done to be able to seed the now single cells, hence being able to observe the cell morphology. The morphology of the seeded cells visualizes a cell structure of differentiated cells as the cells no longer obtained the typical round iPS cell structure. Microscopical analysis of the microtissues made it possible to visualize its ECM. It can be concluded that the microtissue is, in fact, a small tissue of differentiated cells that are producing connective tissue. To evaluate what cell type the iPS cells have differentiated to, the collagen type II synthesis was studied with immunohistochemical staining. The microtissues had produced an amount of collagen type II comparable to the positive control containing chondrocytes. As the collagen type II is predominant in articular cartilage it can be conceivable that the cells have differentiated towards chondrocytes. To provide more evidence and to assure what cell type the iPS cells has differentiated to, immunohistochemical staining of more cartilage specific ECM-components can be conducted.

To 3D bioprint with microtissues instead of single cells is of interest since the micro-

tissues provide an environment for the iPS cells to differentiate. Previous research indicates the possibility of 3D bioprinting with pellets (Gatenholm et al., 2020), see Section 3.1.2.1. As the pellets are cultured in a 96-well plate with 200,000 cells per well these are of a larger volume than the microtissues cultured in microwell culture plates. As the AggreWell^{TM} 800 contains 7200 microwells with 10,000 cells/microwell these microtissues are 20 times smaller in size, thus easier to print than the cell pellets. As many microtissues as possible immersed in the bioink is of interest as the aim is to 3D bioprint a tissue construct.

The real-time quantitative reverse transcription-PCR contributed to a more thorough understanding of the differentiation of the iPS cells that had been cultured as microtissues. The expression of the pluripotency marker OCT4 in the two microtissue-samples as well as in the chondrocyte pellets was extensively low compared to the iPS cells. Accordingly, the cells in the microtissues have differentiated and can no longer be considered as pluripotent. Taken together, the expression of SOX9 and VCAN show that the cells in the microtissues have differentiated toward chondrocytes, yet the production of mature cartilage is not complete. Mentioned cells express SOX9 that is involved in chondrocyte differentiation and novel cartilage formation. The VCAN gene encodes for the proteoglycan Versican that is present in the ECM. The low VCAN expression could indicate that the cells have not yet produced mature cartilage tissue. The variation in expression of collagen type IIB between the two microtissue-samples prevents a reliable evaluation. Collagen type IIB is a splicing variant of the type II procollagen gene that may be expressed in greater amounts in mature cartilage. Hence, the low expression of collagen type IIB in both the microtissues as well as the chondrocyte pellets might be because of the *invitro* culturing that can not be exactly equated with *invivo* cartilage tissue. Analysis of the expression of collagen type IIA or collagen type I would have provided more adequate results for the evaluation of interest. An additional evaluation that would provide further understanding of the cell differentiation is Fluorescence-activated cell sorting (FACS). This method would enable the observation of proteins that have been translated and expressed. FACS could contribute to the evaluation of the differentiation of iPS cells in 3D cell culture.

5.5 Screening for ACAN Induction or Inhibition

The FDA-approved library of small molecules were added continuously to both Plate 1 and Plate 2 during the weeks of screening. The plates were screened every week and images were obtained to be able to compare the results. Some of the wells resulted in an obvious change in fluorescence, thus affected of the molecules. There were wells that visualized an indication of induction as the intensity increased and there were wells showing an inhibition as the intensity decreased. The method is based on visualization of small differences in intensity, hence challenging when comparing the 96 wells at four occasions during the four weeks. Four images of the two plates each were set side by side and correlated to the corresponding well each week.

The difference in intensity was expected to be more obvious and easier to distinguish. Unfortunately, imaging of the two plates before the exposure to the molecules were not obtained which contributed to the challenge of comparing the wells. Due to the absence of these images, the wells indicating induction were especially difficult to analyze. Other options were discussed, such as replicate possibilities for a statistical evaluation. The FDA-approved library of small molecules were evaluated and the possible candidates found were presented and will be submitted to further evaluation. As the modified cell line H8 did not form the same intact microtissue aggregates as the A2B cell line, an interesting analysis would have been to further optimize the H8 microtissues and expose these for the molecules to enable easily interpretable screening.

5.6 Conclusion

To conclude, the current project proves the feasibility of 3D bioprinting cartilaginous tissue with microtissues formed from induced pluripotent stem cells. The formation of microtissues enables the differentiation of induced pluripotent stem cells into mature cells with the ability to produce ECM. Moreover, the study has successfully conducted a comprehensible protocol for the production of an optimized bioink. The bionk, a combination of 60/40 NFC/A (% w/w), possesses the rheological properties required for bioprinting as well as it provides a favorable milieu for the cells. The screening of the FDA-approved library of small molecules resulted in 8 candidate molecules with the capacity of induction and 6 molecules with the capacity of inhibition of aggrecan production. This research will hopefully contribute to the field of 3D bioprinting with iPS cells as a future cure for cartilaginous lesions and OA.

References

Aldrich, S. (2020). *Product Directory Home.* Retrieved 2020-04-08, from https://www.sigmaaldrich.com/technical-service-home/product-catalog.html

Arthritis Foundation. (2017). *Osteoarthritis.* Retrieved 2020-02-11, from https://www.arthritis.org/diseases/osteoarthritis

Artros.org. (2019). *Artros i Sverige - Så vanligt förekommande är ledsjukdomen.* Retrieved 2020-02-10, from https://www.artros.org/fakta-om-artros/artros-i-sverige/

BIO X - CELLINK. (2020). Retrieved 2020-05-19, from https://www.cellink.com/product/cellink-bio-x/

Boreström, C., Simonsson, S., Enochson, L., Bigdeli, N., Brantsing, C., Ellerström, C., ... Lindahl, A. (2014). Footprint-Free Human Induced Pluripotent Stem Cells From Articular Cartilage With Redifferentiation Capacity: A First Step Toward a Clinical-Grade Cell Source. *STEM CELLS Translational Medicine*, *3*(4), 433–447. doi: 10.5966/sctm.2013-0138

Cardoso, D. A., Ulset, A. S., Bender, J., Jansen, J. A., Christensen, B. E., & Leeuwenburgh, S. C. (2014). Effects of physical and chemical treatments on the molecular weight and degradation of alginate-hydroxyapatite composites. *Macromolecular Bioscience*, *14*(6), 872–880. doi: 10.1002/mabi.201300415

Dahlin, R. L., Ni, M., Meretoja, V. V., Kasper, F. K., & Mikos, A. G. (n.d., jan). TGF-β3-induced chondrogenesis in co-cultures of chondrocytes and mesenchymal stem cells on biodegradable scaffolds. *Biomaterials*(1), 123–32. doi: 10.1016/j.biomaterials.2013.09.086

Doral, M. N., Bilge, O., Huri, G., Turhan, E., & Verdonk, R. (n.d.). Modern treatment of meniscal tears. *EFORT Open Reviews*(5), 260–268. doi: 10.1302/2058-5241.3.170067

Enochson, L., Brittberg, M., & Lindahl, A. (n.d.). Optimization of a Chondrogenic Medium Through the Use of Factorial Design of Experiments. *BioResearch*

Open Access(6), 306. doi: 10.1089/BIORES.2012.0277

Gatenholm, B., Lindahl, C., Brittberg, M., & Simonsson, S. (2020). Collagen 2A Type B Induction after 3D Bioprinting Chondrocytes In Situ into Osteoarthritic Chondral Tibial Lesion. *Cartilage*. doi: 10.1177/1947603520903788

Gibco. (2014). *Gibco™ Insulin-Transferrin-Selenium (ITS -G) (100X)*. Retrieved 2020-04-06, from `https://www.fishersci.co.uk/shop/products/gibco-insulin-transferrin-selenium-its-g-100x/12097549`

Gille, J., Behrens, P., Schulz, A. P., Oheim, R., & Kienast, B. (2016). Matrix-Associated Autologous Chondrocyte Implantation. *CARTILAGE*(4), 309–315. doi: 10.1177/1947603516638901

Gobbi, A., & Lane, J. G. (2017). *Bio-orthopaedics A New Approach*. Retrieved from `https://www.springer.com/gp/book/9783662541807`

Huang, K., & Wu, L. D. (2008). *Aggrecanase and Aggrecan Degradation in Osteoarthritis: a Review* (Vol. 36; Tech. Rep.). doi: 10.1177/147323000803600601

Jarit, G. J., & Bosco, J. A. (2010). Meniscal repair and reconstruction. *Bulletin of the NYU Hospital for Joint Diseases*, *68*(2), 84–90.

Kawata, M., Sasabuchi, Y., Taketomi, S., Inui, H., Matsui, H., Fushimi, K., ... Tanaka, S. (2018). Annual trends in arthroscopic meniscus surgery: Analysis of a national database in Japan. *PloS one*, *13*(4), e0194854. doi: 10.1371/journal.pone.0194854

Li, J., Chen, M., Fan, X., & Zhou, H. (2016). Recent advances in bioprinting techniques: approaches, applications and future prospects. *Journal of translational medicine*, *14*, 271. doi: 10.1186/s12967-016-1028-0

Makris, E. A., Hadidi, P., & Athanasiou, K. A. (2011). The knee meniscus: structure-function, pathophysiology, current repair techniques, and prospects for regeneration. *Biomaterials*, *32*(30), 7411–31. doi: 10.1016/j.biomaterials.2011.06.037

Maldonado, M., & Nam, J. (2013). The role of changes in extracellular matrix of cartilage in the presence of inflammation on the pathology of osteoarthritis. *BioMed research international*, *2013*, 284873. doi: 10.1155/2013/284873

Markstedt, K., Mantas, A., Tournier, I., Martínez Ávila, H., Hägg, D., & Gatenholm, P. (2015). 3D bioprinting human chondrocytes with nanocellulose-alginate bioink for cartilage tissue engineering applications. *Biomacromolecules*, *16*(5),

1489–1496. doi: 10.1021/acs.biomac.5b00188

Medvedev, S. P., Shevchenko, A. I., & Zakian, S. M. (2010). Induced Pluripotent Stem Cells: Problems and Advantages when Applying them in Regenerative Medicine. *Acta naturae*, *2*(2), 18–28.

Nguyen, D., Hgg, D. A., Forsman, A., Ekholm, J., Nimkingratana, P., Brantsing, C., ... Simonsson, S. (2017). Cartilage Tissue Engineering by the 3D Bioprinting of iPS Cells in a Nanocellulose/Alginate Bioink. *Scientific Reports*, *7*(1), 1–10. doi: 10.1038/s41598-017-00690-y

Ortho Center Skåne. (2011). *Meniskskada - Ortho Center Skåne.* Retrieved 2020-02-27, from `https://skane.orthocenter.se/behandlingar/kna/meniskskada` doi: https://skane.orthocenter.se/behandlingar/kna/meniskskada

Papaioannou, T. G., Manolesou, D., Dimakakos, E., Tsoucalas, G., Vavuranakis, M., & Tousoulis, D. (2019). 3D Bioprinting Methods and Techniques: Applications on Artificial Blood Vessel Fabrication. *Acta Cardiologica Sinica*, *35*(3), 284. doi: 10.6515/ACS.201905_35(3).20181115A

Poole, A. R., Kojima, T., Yasuda, T., Mwale, F., Kobayashi, M., & Laverty, S. (2001). Composition and structure of articular cartilage: A template for tissue repair. *Clinical Orthopaedics and Related Research*(391 SUPPL.). doi: 10.1097/00003086-200110001-00004

Roughley, P. J., & Mort, J. S. (2014). The role of aggrecan in normal and osteoarthritic cartilage. *Journal of Experimental Orthopaedics*, *1*(1), 1–11. doi: 10.1186/s40634-014-0008-7

Sanchez-Adams, J., & Athanasiou, K. A. (2012). Biomechanics of Meniscus Cells: Regional Variation and Comparison to Articular Chondrocytes and Ligament Cells.
doi: 10.1007/s10237-012-0372-0

Semba, J. A., Mieloch, A. A., & Rybka, J. D. (2020). Introduction to the state-of-the-art 3D bioprinting methods, design, and applications in orthopedics. *Bioprinting*, *18*(September 2019), e00070. doi: 10.1016/j.bprint.2019.e00070

Sophia Fox, A. J., Bedi, A., & Rodeo, S. A. (2009). The basic science of articular cartilage: Structure, composition, and function. *Sports Health*, *1*(6), 461–468. doi: 10.1177/1941738109350438

Strauss, E. J., Barker, J. U., Kercher, J. S., Cole, B. J., & Mithoefer, K. (2010). Augmentation Strategies following the Microfracture Technique for Repair of Focal Chondral Defects. *CARTILAGE*, *1*(2), 145–152. doi: 10.1177/1947603510366718

Takahashi, K., Tanabe, K., Ohnuki, M., Narita, M., Ichisaka, T., Tomoda, K., & Yamanaka, S. (2007). Induction of Pluripotent Stem Cells from Adult Human Fibroblasts by Defined Factors. *Cell*, *131*(5), 861–872. doi: 10.1016/j.cell.2007.11.019

Takahashi, K., & Yamanaka, S. (2006). Induction of Pluripotent Stem Cells from Mouse Embryonic and Adult Fibroblast Cultures by Defined Factors. *Cell*, *126*(4), 663–676. doi: 10.1016/j.cell.2006.07.024

Thomson, J. A., Itskovitz-Eldor, J., Shapiro, S. S., Waknitz, M. A., Swiergiel, J. J., Marshall, V. S., ... Thomson, J. A. (1998, nov). Embryonic stem cell lines derived from human blastocysts. *Science (New York, N.Y.)*, *282*(5391), 1145–7. Retrieved from `http://www.ncbi.nlm.nih.gov/pubmed/9804556` doi: 10.1126/science.282.5391.1145

Wang, Y., Wei, L., Zeng, L., He, D., & Wei, X. (2013). Nutrition and degeneration of articular cartilage. *Knee Surgery, Sports Traumatology, Arthroscopy*, *21*(8), 1751. doi: 10.1007/S00167-012-1977-7